J. Fluid Mech. (2005), *vol.* 533, *pp.* 95–124.
doi:10.1017/S0022112005004064 Printed in the United Kingdom

On compound liquid threads with large viscosity contrasts

By R. V. CRASTER[1], O. K. MATAR[2] AND D. T. PAPAGEORGIOU[3]

[1]Department of Mathematics, Imperial College London SW7 2AZ, UK

[2]Department of Chemical Engineering, Imperial College London SW7 2AZ, UK

[3]Department of Mathematical Sciences, and Center for Applied Mathematics and Statistics, New Jersey Institute of Technology, University Heights, Newark, NJ 07102, USA

(Received 16 December 2003 and in revised form 29 November 2004)

Compound viscous jets composed of an inner core of one fluid surrounded by an annulus of another are studied here using long-wave theory. We investigate the limit of strongly differing viscosities in the neighbouring fluids: either a highly viscous core or annulus. Additionally, if inertia is present, the density ratio of the fluids is assumed to mirror that of the viscosities. The resulting asymptotic theory reduces to several earlier theories in the appropriate limits. Linear stability analysis and full numerical simulations of the one-dimensional set of equations allow an exploration of the dynamics of either the interior or exterior fluid. The results of our linear stability analysis demonstrate that, for both cases, a stretching and a squeezing mode exist, with the former being more dominant than the latter. Our numerical simulations show that in the highly viscous core case, the interfaces can move out-of-phase, leading to the breakup of the annular region; this is contrary to the linear theory predictions. In the highly viscous annulus case, our results demonstrate the possibility of breakup of either the core or the annulus, depending on the initial ratio of the radii.

1. Introduction

Compound jets and threads composed of a core liquid surrounded by an annular layer of another immiscible liquid (see figure 1) form an important class of flows particularly in areas that involve particle sorting, fibre-spinning, micro-encapsulation in foods, drug delivery, ink-jet printing, and materials science applications (Herzenberg & Sweet 1976; Denn 1980; Hertz & Hermanrud 1983; Mathiowitz *et al.* 1997; Hardas *et al.* 2000; Jung *et al.* 2000; Burlak *et al.* 2001; Lee *et al.* 2001). These compound threads that feature an inner and an outer interface (if the annular layer is bounded by, say, an inviscid gas) are susceptible to a surface tension-induced instability, that ultimately leads to their breakup into drops of varying sizes.

The subject of single-jet breakup has received considerable attention in the literature starting with the early theoretical work of Lord Rayleigh (1878), who showed, using a temporal stability analysis for an inviscid doubly infinite jet, that perturbations of wavelength larger than the undisturbed jet circumference grow and lead to breakup into droplets – linear theory provides theoretical predictions which are in surprisingly good agreement with experiments (for a recent experimental study see Chauhan *et al.* (2003) and references therein). The effect of viscosity and a surrounding viscous phase was introduced by Tomotika (1934) and Chandrasekhar (1961), and a considerable

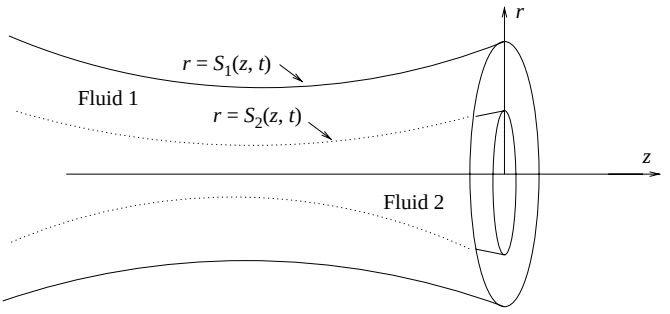

FIGURE 1. Schematic representation of a compound thread.

body of work has developed regarding the linear stability of capillary jet flows (see reviews by Denn 1980; Eggers 1997; Lin & Reitz 1998). Viscosity does not change the qualitative features of the instability, but merely reduces maximum growth rates and elongates the length of the most unstable waves.

The temporal stability model assumes an initial condition and solves for the large-time behaviour of the system. Since disturbances are usually introduced at the jet nozzle and are maintained throughout an experiment (or in applications through natural vibrations of the nozzle, for example), it was suggested by Keller, Rubinow & Tu (1973) that a spatial stability allowing growth of disturbances with axial position, may be more appropriate and indeed find spatial instability if the Weber number (the ratio of inertial to capillary pressure) is above a threshold value. This problem was analysed further by Leib & Goldstein (1986*a*, *b*) who find absolute instability below a threshold Weber number.

The nonlinear stability of single jets has received much attention starting with the work of Lee (1974), who used a one-dimensional model to predict inviscid capillary jet breakup; see also Schulkes (1993*a*, *b*) for a more modern treatment. The success of one-dimensional models in describing breakup of viscous jets, has emerged from several investigations including those of Eggers & Dupont (1994), Eggers (1995, 1997) and Papageorgiou (1995*a*, *b*). The approach is to analyse simpler models and predict singular structures by constructing local similarity solutions. Of particular interest are experimental verifications of the highly viscous (Stokes) theory of Papageorgiou (1995*a*, *b*) by McKinley & Tripathi (2000) and Rothert, Richter & Rehberg (2003) who also consider the viscous–inertial regime of Eggers (see also the studies of Brenner, Shi & Nagel 1994; Shi, Brenner & Nagel 1994; Lister & Stone 1998; Wilkes, Phillips & Basaran 1999; Notz, Chen & Basaran 2001; Chen, Notz & Basaran 2002).

An important issue is how well these one-dimensional models compare both with experiments and full numerical simulations of the Navier–Stokes equations, particularly as some overturning of the interface occurs (Wilkes *et al.* 1999) for a drop falling under gravity. Ambravaneswaran, Wilkes & Basaran (2002) carefully compare and extend the models showing that the one-dimensional models perform adequately. Indeed, one motivation for the current long-wave theory is to build a more general model that encompasses the high-viscosity contrasts sometimes seen in experiments (see Doshi *et al.* 2003).

In contrast to the single-fluid jet, compound jets have received less attention. One of the first studies was the experimental work of Hertz & Hermanrud (1983) who demonstrated the feasibility of compound drop formation with applications in ink-jet technologies. Sanz & Meseguer (1985) and Radev & Shkadov (1985) considered the

linear stability of inviscid compound jets based on one-dimensional approximations, and viscosity was included in the linear stability by Radev & Tchavdarov (1988) and Shkadov & Sisoev (1996) (also in a one-dimensional approximation). It is established in these studies that there are two unstable modes present: a *stretching mode* where the two interfaces grow in-phase, and a *squeezing mode* with the interfaces growing exactly out-of-phase. The former instability sets the conditions for possible breakup of the inner thread first followed by the outer interface (leading to encapsulation), while the latter can produce breakup of the annular layer first and thus de-wetting of the central core fluid. (In the present study, we present nonlinear solutions based on one-dimensional models that capture both phenomena.) The linear studies find that the stretching mode is the dominant one; viscosity does not qualitatively change these results. The spatial stability of an inviscid compound jet was carried out by Chauhan *et al.* (1996) who find two spatially unstable modes; they also extended the large Weber number asymptotic analysis of Keller *et al.* (1973), to a compound jet. A more complete stability study of the viscous compound jet was performed by Chauhan *et al.* (2000) who considered a whole range of parameter values (e.g. viscosity, density, surface tension and inner to outer radii ratios) and found that the stretching mode retains its dominance, at least throughout the linear regime. A physical interpretation of this is that the stretching mode releases energy from both interfaces, whereas the squeezing mode only releases energy from one and thus grows more slowly.

The effect of surfactants on the stability of single and compound threads has been considered by Ambravaneswaran & Basaran (1999), Hansen, Peters & Meijer (1999), Kwak & Pozrikidis (2001), Timmermans & Lister (2002) and Craster, Matar & Papageorgiou (2002). The latter study involved the derivation of a coupled set of evolution equations for the interfacial location, the surfactant concentration and the axial velocity component using long-wave theory. In that work, it was shown that although the presence of surfactant does not alter the behaviour near pinching from the similarity solution of Eggers (1993), it does rigidify the interface, leading to the formation of smaller satellite drops. This is because the surfactant lowers the mean value of the surface tension and gradients in surfactant concentration give rise to Marangoni stresses, which counteract the surface-tension-induced breakup.

Craster, Matar & Papageorgiou (2003) (hereinafter referred to as paper I) then extended this long-wave theory to cover surfactant-laden compound threads featuring fluids of comparable viscosity. One feature that emerges from the long-wave theory is that the axial velocity field is independent of the radial coordinate, and hence is common to both fluids. This leads to the synchronization of the two fluid interfaces and we can deduce a rescaling that, in most cases, reduces the two-fluid system to an effective single-fluid thread, which has been extensively studied. The aim of the present paper is to move beyond this situation and consider viscosity differences that are more pronounced, leading to a radially dependent axial velocity component (Henson, Cao & Bechtel 1998). This, then, permits the breakup of either the inner or outer phase depending on the magnitude of the relevant system parameters. Thus this asymptotic theory can capture more realistic and varied dynamics than that presented in paper I. Note that surfactant effects will not be considered here.

There are two different situations to consider: a highly viscous fluid core surrounded by a much less viscous fluid annulus and a highly viscous annulus surrounding a much less viscous core. We also assume that the ratio of fluid densities is the same as that of the viscosities. This is done primarily to ensure that our derived equations reduce to other equations that describe the evolution of threads and jets in the literature, although we acknowledge the difficulty of finding a pair of fluids such that the more

viscous fluid is also the denser of the two. Long-wave theory will be used in order to derive the relevant set of evolution equations by exploiting the viscosity ratio in each case; this will serve as the parameter allowing the construction of an asymptotic theory featuring a radially dependent axial velocity. The stability of the threads is then considered in both the linear and nonlinear regimes, and predictions regarding the likelihood of breakup of the inner and outer phases will be made as a function of system parameters by using accurate computations.

The rest of this paper is organized as follows: We give a detailed formulation of the highly viscous core and annulus cases, followed by sections on linear theory and numerical simulations of the nonlinear evolution equations. Concluding remarks are given in § 5.

2. Problem formulation

Here, we present details of the derivation of the coupled sets of partial differential equations governing the evolution of the threads. We consider the highly viscous core first, followed by that of a highly viscous annulus.

2.1. *Highly viscous core*

We construct a theory for the evolution of an axisymmetric compound jet comprising a highly viscous core, of radius $r = S_2(z,t)$, surrounded by a much less viscous annulus of radius $r = S_1(z,t)$ (see figure 1). The subscripts '1' and '2' are hereinafter used to denote properties associated with these two radii, and to distinguish the outer and inner fluids, respectively.

The annular (core) fluid has viscosity μ_1 (μ_2) and density ρ_1 (ρ_2) with the interfaces at $r = S_1$ (S_2) having constant surface tensions σ_1 (σ_2). These fluids are considered to be Newtonian and incompressible and $\mu_1 \ll \mu_2$. The compound thread is surrounded by air, which is taken to be inviscid. We use a cylindrical coordinate system (r, θ, z), with corresponding velocity field $(u, 0, w)$, to describe the dynamics of the annular region, $S_2(z,t) \leqslant r \leqslant S_1(z,t)$, and of the core region, $0 \leqslant r \leqslant S_2(z,t)$. The governing equations are the usual Navier–Stokes equations and mass conservation in each fluid region. These are coupled by stress and velocity conditions.

We begin by non-dimensionalizing using the initial radius of the core region, $\mathscr{R}$, as the characteristic dimension of r, and $\mathscr{L}$ as a characteristic horizontal length scale; the aspect ratio $\epsilon = \mathscr{R}/\mathscr{L}$ plays an important role as it provides the small parameter that is used in the analysis. Furthermore, we measure the speed u by $\mathscr{V} = \sigma_2/\mu_2$, w by $\mathscr{L}\sigma_2/\mathscr{R}\mu_2$, time by $\mathscr{R}/\mathscr{V}$ and the pressures p_i by $\sigma_2/\mathscr{R}$. The non-dimensional governing equations in the annular region are then expressed by:

$$l\,Re\left(u_{1_t} + u_1 u_{1_r} + w_1 u_{1_z}\right) = -p_{1_r} + m\left(\frac{1}{r}[r u_{1_r}]_r - \frac{u_1}{r^2} + \epsilon^2 u_{1_{zz}}\right), \tag{2.1}$$

$$l\,Re\left(w_{1_t} + u_1 w_{1_r} + w_1 w_{1_z}\right) = -\epsilon^2 p_{1_z} + m\left(\frac{1}{r}[r w_{1_r}]_r + \epsilon^2 w_{1_{zz}}\right), \tag{2.2}$$

$$\frac{1}{r}(r u_1)_r + w_{1_z} = 0. \tag{2.3}$$

Here, viscosity and density ratios emerge, given by $m \equiv \mu_1/\mu_2$ and $l \equiv \rho_1/\rho_2$, respectively, in addition to a Reynolds number, $Re \equiv \rho_2 \mathscr{V} \mathscr{R}/\mu_2$.

In the core region, we have

$$Re\left(u_{2_t} + u_2 u_{2_r} + w_2 u_{2_z}\right) = -p_{2_r} + \left(\frac{1}{r}[r u_{2_r}]_r - \frac{u_2}{r^2} + \epsilon^2 u_{2_{zz}}\right), \tag{2.4}$$

$$Re\left(w_{2_t} + u_2 w_{2_r} + w_2 w_{2_z}\right) = -\epsilon^2 p_{2_z} + \left(\frac{1}{r}[r w_{2_r}]_r + \epsilon^2 w_{2_{zz}}\right), \tag{2.5}$$

$$\frac{1}{r}(r u_2)_r + w_{2_z} = 0. \tag{2.6}$$

The normal and shear stress balances at the outer interface, $r = S_1$, are given by

$$p_1 - \frac{2m}{1+\epsilon^2 S_{1_z}^2}\left(u_{1_r} - S_{1_z}\left[\epsilon^2 u_{1_z} + w_{1_r}\right] + \epsilon^2 S_{1_z}^2 w_{1_z}\right) = \gamma\left(\frac{1}{S_1} - \epsilon^2 S_{1_{zz}}\right), \tag{2.7}$$

$$m\left[\left(1-\epsilon^2 S_{1_z}^2\right)\left(w_{1_r} + \epsilon^2 u_{1_z}\right) + 2\epsilon^2 S_{1_z}\left(u_{1_r} - w_{1_z}\right)\right] = 0. \tag{2.8}$$

We note (this is adopted in the remainder of the paper also) that the full curvature term on the right-hand side of (2.7) is given by $(1+\epsilon^2 S_{1_z}^2)^{1/2}/S_1 - \epsilon^2 S_{1_{zz}}/(1+\epsilon^2 S_{1_z}^2)^{1/2}$, and for simplicity we model this with order ϵ^2 accuracy. This provides an appropriate regularization of high wavenumbers which is useful in the computations, without affecting singularity structures. (For a comparative study of different models in inviscid flows where the approximation of the curvature term can matter, see Papageorgiou & Orellana (1998); see also Ambaravaneswaran *et al.* (2002) for a comparison of the predictions of one- and two-dimensional models.)

The parameter γ that emerges is a ratio of surface tensions, $\gamma = \sigma_1/\sigma_2$. At the inner interface, $r = S_2$, the equivalent balances are given by

$$p_2 - \frac{2}{\left(1+\epsilon^2 S_{2_z}^2\right)}\left(\epsilon^2 S_{2_z}^2 w_{2_z} - S_{2_z}\left(\epsilon^2 u_{2_z} + w_{2_r}\right) + u_{2_r}\right)$$
$$-\left(p_1 - \frac{2m}{\left(1+\epsilon^2 S_{2_z}^2\right)}\left(\epsilon^2 S_{2_z}^2 w_{1_z} - S_{2_z}\left(\epsilon^2 u_{1_z} + w_{1_r}\right) + u_{1_r}\right)\right) = \left(\frac{1}{S_2} - \epsilon^2 S_{2_{zz}}\right), \tag{2.9}$$

$$\left[\left(1-\epsilon^2 S_{2_z}^2\right)\left(\epsilon^2 u_{2_z} + w_{2_r}\right) + 2\epsilon^2 S_{2_z}\left(u_{2_r} - w_{2_z}\right)\right]$$
$$- m\left[\left(1-\epsilon^2 S_{2_z}^2\right)\left(\epsilon^2 u_{1_z} + w_{1_r}\right) + 2\epsilon^2 S_{2_z}\left(u_{1_r} - w_{1_z}\right)\right] = 0. \tag{2.10}$$

Additionally, there are kinematic boundary conditions for the interface positions S_1, S_2 given by

$$S_{i_t} + w_i S_{i_z} = u_i \qquad (i = 1, 2). \tag{2.11}$$

2.1.1. *Asymptotic reduction*

We perform an asymptotic reduction of this set of equations in the limit of small ϵ, which corresponds to long and thin threads. Here, the aim is to capture the essential physics within a simpler set of equations. Furthermore, to model high-viscosity contrasts, we set the viscosity and density ratios to $m = \epsilon^2 M$ and $l = \epsilon^2 L$. This choice for the density ratio has the effect of explicitly removing L from the subsequent theory, and we are therefore additionally assuming that the highly viscous fluid is more dense than the less viscous one. The density ratio can be further relaxed to $l = \epsilon L$; the role of this density choice is to ensure that the inertial term in the axial component of the Navier–Stokes equations for the less viscous fluid does not enter at leading order, thereby enabling analytical progress to be made. This allows

us to retain inertial contributions in the more viscous of the two fluids in the final equations which, as will be shown below, allows us to recover other equations in the literature from our equations by taking appropriate limits. Note that an alternative approach would have involved the solution of the Stokes flow problem in both fluids. This would have obviated the need to make assumptions regarding the magnitude of l.

We also rescale the Reynolds number such that $Re = \epsilon^2 \overline{Re}$; this scaling for the Reynolds number is usually adopted for viscous threads and jets and ensures that inertia enters also to leading order (Craster *et al.* 2002). We note that $\gamma = O(1)$ and that the scaling $m \sim \epsilon^2$ provides the canonical asymptotic limit for which a radial dependence is seen in the leading-order axial velocity (see below); this is a new feature compared to the $m = O(1)$ case analysed in paper I where a plug flow is obtained for the leading-order axial velocity throughout the compound jet. We introduce the expansions $w_1 = w_1^{(1)} + \epsilon^2 w_1^{(2)} + \ldots$, with similar expressions for the other dependent variables (the expansion proceeds in powers of ϵ^2 owing to its natural occurrence in all the governing equations and boundary conditions) and drop the superscripts '1' from the leading-order equations to obtain the following leading-order radial and axial components of the Navier–Stokes equations in the annular region:

$$p_{1_r} = 0, \quad p_{1_z} = \frac{M}{r}\left(r w_{1_r}\right)_r, \tag{2.12}$$

whence, $p_1 = p_1(z,t)$ only (to be given by the normal stress balance at $r = S_1$) and the leading-order axial velocity component in this region is

$$w_1 = \frac{1}{M}\left(p_{1_z}\frac{r^2}{4} - c_1(z,t)\ln r - c_2(z,t)\right). \tag{2.13}$$

Using the continuity equation we determine the leading-order radial velocity component in this region to be:

$$u_1 = -\frac{1}{M}\left(p_{1_{zz}}\frac{r^3}{16} - \frac{r}{2}c_{2_z} - c_{1_z}\frac{r}{2}\ln r + c_{1_z}\frac{r}{4}\right) + \frac{c_3(z,t)}{r}. \tag{2.14}$$

Here $c_i(z,t)$ for $i = 1, \ldots, 3$ are, at present, unknown functions and we now analyse the governing equations further in order to deduce them.

The leading-order normal stress balance at $r = S_1$ yields the pressure distribution in the annular region:

$$p_1 = \gamma\kappa_1, \tag{2.15}$$

in which the curvature, κ_1, is given by

$$\kappa_1 = \frac{1}{S_1} - \epsilon^2 S_{1_{zz}}. \tag{2.16}$$

Note that we have retained a seemingly *ad hoc* correction to the curvature of $O(\epsilon^2)$ that acts to introduce a high wavenumber cutoff and aids numerical computations.

Substitution of (2.13) into the leading-order shear stress balance at $r = S_1$, given by

$$w_{1_r} = 0, \tag{2.17}$$

yields an expression for $c_1(z,t)$:

$$c_1(z,t) = \tfrac{1}{2}S_1^2 p_{1_z}. \tag{2.18}$$

The leading-order axial component of the Navier–Stokes equations in the core is

$$\frac{1}{r}\left(r w_{2_r}\right)_r = 0. \tag{2.19}$$

Recalling that we require boundedness at $r = 0$, the leading-order axial velocity in the core is then given by $w_2 \equiv w_2(z,t)$. Thus the leading-order axial velocity component in the core is independent of the radial coordinate much as in the conventional single-fluid jet analysis (Papageorgiou 1995*a*, *b*).

Using continuity, the leading-order radial velocity component in the core is determined to be

$$u_2 = -w_{2_z}\frac{r}{2}. \tag{2.20}$$

Substitution of (2.20) into the leading-order radial component of the Navier–Stokes equations in the core region yields $p_{2_r} = 0$, implying that $p_2 \equiv p_2(z,t)$ and it is given by the leading-order normal stress balance in this region:

$$p_2 = p_1 - w_{2_z} + \kappa_2 = \gamma\left(\frac{1}{S_1} - \epsilon^2 S_{1_{zz}}\right) + \left(\frac{1}{S_2} - \epsilon^2 S_{2_{zz}}\right) - w_{2_z}. \tag{2.21}$$

The leading-order shear stress balance in this region is $w_{2_r} = 0$, which is already satisfied.

Demanding continuity of the axial and radial velocity components at $r = S_2$ yields

$$c_2(z,t) = p_{1_z}\frac{S_2^2}{4} - c_1 \ln S_2 - M w_2, \tag{2.22}$$

and

$$c_3(z,t) = -\frac{w_{2_z}}{2}S_2^2 + \frac{1}{M}\left(p_{1_{zz}}\frac{S_2^4}{16} - \frac{S_2^2}{2}c_{2_z} + c_{1_z}\frac{S_2^2}{2}\left(\tfrac{1}{2} - \ln S_2\right)\right). \tag{2.23}$$

Thus, at this stage, only w_2 must be determined in order to derive the leading-order equations.

To make further progress we examine the second-order axial component of the Navier–Stokes equations in the core region:

$$\overline{Re}(w_{2_t} + w_2 w_{2_z}) = -p_{2_z} + \left[\frac{1}{r}\left(r w_{2_r}^{(2)}\right)_r + w_{2_{zz}}\right], \tag{2.24}$$

in which $w_2^{(2)}$ represents the second-order contribution to the axial velocity component in the core. Integration of this equation, and using boundedness at $r = 0$, yields

$$w_{2_r}^{(2)} = \tfrac{1}{2} r\left[\overline{Re}\left(w_{2_t} + w_2 w_{2_z}\right) + p_{2_z} - w_{2_{zz}}\right]. \tag{2.25}$$

Substitution of (2.25) into the second-order shear stress balance at $r = S_2$, which is given by

$$w_{2_r}^{(2)} + u_{2_z} + 2S_{2_z}(u_{2_r} - w_{2_z}) - M w_{1_r} = 0, \tag{2.26}$$

yields the following evolution equation for $w_2(z,t)$:

$$\overline{Re}\left(w_{2_t} + w_2 w_{2_z}\right) = \frac{3}{S_2^2}\left(S_2^2 w_{2_z}\right)_z - (\kappa_2)_z - \gamma\left(\frac{S_1}{S_2}\right)^2(\kappa_1)_z. \tag{2.27}$$

Together with evolution equations for S_2 and S_1, that are the kinematic conditions at the interfaces,

$$S_{2_t} + w_2 S_{2_z} + \frac{S_2}{2}w_{2_z} = 0, \tag{2.28}$$

$$S_{1_t} + w_1(S_1, z, t)S_{1_z} = u_1(S_1, z, t), \tag{2.29}$$

we now have a closed system of evolution equations for the thread dynamics. The functions $w_1(S_1, z, t)$, $u_1(S_1, z, t)$ and $w_{1_z}(S_1, z, t)$ are given by (2.13), (2.14), (2.18), (2.22) and (2.23). Note that the dependence of (2.27)–(2.29) upon the Reynolds number can be removed via the rescaling

$$S_i \to \overline{Re}\, S_i, \quad ()_t \to \frac{1}{\overline{Re}}()_t, \quad w_i \to w_i/\overline{Re}. \tag{2.30}$$

The governing system (2.27)–(2.29) conserves momentum and mass, as we briefly outline next. Using the leading-order curvatures $\kappa_1 = 1/S_1$ and $\kappa_2 = 1/S_2$, we multiply equation (2.27) by $S_2^2/2$, and (2.28) by $\overline{Re}\, S_2 w_2$ and add to obtain

$$\left(S_2^2 w_2\right)_t + \left(S_2^2 w_2^2\right)_z = \mathscr{F}_z, \tag{2.31}$$

where $\mathscr{F}$ is a known function we need not give here. It follows that $\int S_2^2 w_2 \, \mathrm{d}z$ is a conserved quantity and is proportional to the total momentum of region 2. (For definiteness we consider periodic domains as is done in the simulations that follow.)

Mass conservation in region 2 follows trivially by multiplication of (2.28) by S_2. To derive an analogous result for region 1, multiply (2.29) by S_1 to obtain

$$\left(S_1^2\right)_t + 2\left(S_1 S_{1_z} w_1 - S_1 u_1\right) = 0. \tag{2.32}$$

It is enough to show that $S_1 S_{1_z} w_1 - S_1 u_1$ can be written as $\mathscr{G}_z$ for some function $\mathscr{G}$, in which case mass conservation follows by integration and periodicity. To achieve this we use the definitions of $w_1(S_1, z, t)$ and $u_1(S_1, z, t)$ using (2.13) and (2.14) and write $c_3(z, t)$ in terms of c_1 and c_2 according to (2.23). After some algebra, we find

$$\begin{aligned} S_1 S_{1_z} w_1 - S_1 u_1 = {} & \frac{1}{8M}\left(p_{1_z} S_2^4\right)_z - \frac{1}{2M}\left(c_2 S_1^2\right)_z \\ & - \frac{1}{2M}\left[c_1\left(S_1^2 \ln S_1 - \tfrac{1}{2} S_1^2\right)\right]_z - \frac{1}{4M}\left(c_1 S_2^2\right)_z, \end{aligned} \tag{2.33}$$

and since the right-hand side is the derivative of a periodic function the required result follows.

2.1.2. *Connections with previous models*

In the limit $M \to \infty$, $c_1 = c_3 = 0$ and $c_2 = -M w_2$, whence $u_1 = -r w_{2_z}/2$ and $w_1 = w_2 = w$. Thus the evolution equations become

$$w_t + w w_z = \frac{3}{S_2^2}\left(S_2^2 w_z\right)_z - (\kappa_2)_z - \gamma\left(\frac{S_1}{S_2}\right)^2 (\kappa_1)_z, \tag{2.34}$$

$$S_{i_t} + w S_{i_z} + \tfrac{1}{2} S_i w_z = 0 \qquad (i = 1, 2). \tag{2.35}$$

This is the system of equations studied in paper I which involved liquids of comparable viscosities and densities. Note that setting $\gamma = 0$ renders the outer fluid passive and $S_2 = S$ recovers the single jet equations studied by Eggers (1993).

Another limit is that of a very thin viscous film exterior to a rigid fibre; the equation derived by Hammond (1983) in his study of annular viscous films on the inside of cylindrical pipes can also be derived from (2.27), (2.28) and (2.29). It is notable that Hammond's work involves flow on the interior of a circular cylinder and as such it is at first glance more akin to the highly viscous annulus we consider next. However, as noted by, for instance, Kalliadasis & Chang (1994), Hammond's equation (2.39) holds in the limit of a very thin annular film on the outside of a fibre; here the interior core has become so viscous that it is, in this limit, effectively rigid.

To recover Hammond's equation, we set $M \ll 1$ to obtain $S_2 \sim 1$, $w_2 \sim 0$ and define the film thickness between S_1 and S_2, h, to be

$$h = \frac{S_1 - 1}{\delta S_1}, \tag{2.36}$$

where $\delta \ll 1$. This reflects the physical situation in the work of Hammond (1983), wherein the film thickness is much smaller than the pipe radius and the viscosity of the film far exceeds that of the core fluid. In this case, u_1 and w_1 evaluated at S_1 are given by

$$u_1 \approx \frac{\delta^3}{6M}\left(3h^2 h_z p_{1_z} + 2h^3 p_{1_{zz}}\right), \tag{2.37}$$

$$w_1 \approx -\frac{\delta^2}{2M} h^2 p_{1_z}, \tag{2.38}$$

in which $p_{1_z} = -\gamma\delta(h_z + \epsilon^2 h_{zzz})$ and $p_{1_{zz}} = -\gamma\delta(h_{zz} + \epsilon^2 h_{zzzz})$. Substitution of u_1, w_1, p_{1_z} and $p_{1_{zz}}$ into (2.29), with $M = \delta^3$, together with the rescaling $t = \hat{t}/\gamma$ yields the following equation for h

$$h_{\hat{t}} = -\tfrac{1}{3}(h^3(h_z + \epsilon^2 h_{zzz}))_z. \tag{2.39}$$

This is in agreement with (3.44) in the work of Hammond (1983) if we further set $\epsilon = 1$. Notably, the choice of scalings and small parameters alter slightly between the articles justifying the choice $\epsilon = 1$, because $\delta \ll \epsilon$ is a small parameter that measures the amplitude of the annular interface; the length of the waves scales with the undisturbed core radius (the pipe radius in Hammond's case) and is long compared to the interfacial deflection.

We were not able to recover the equations of Lister & Stone (1998) as a limiting form of our evolution equations. In our notation, Lister & Stone (1998) have $m = \epsilon^2 \ln(1/\epsilon)$, and hence this limit can be approached by considering $M \to \infty$ and $S_1 \gg S_2$. As shown already, the limit $M \to \infty$ captures the order one viscosity ratio system of paper I, and misses the intermediate case of large but asymptotically smaller M that is necessary for the Lister & Stone (1998) model. Another observation is that the tangential stress balance equation (2.27), at zero Reynolds number, is missing the external drag term on the thread owing to the surrounding medium that forms a central feature of the Lister & Stone (1998) model, and so the present model cannot tend to those limiting forms. It may be possible to achieve this by considering different asymptotic scales for m as was done by Lister & Stone (1998), but this is not pursued further here.

2.2. *Highly viscous annulus*

Here we consider the opposite limit whereby we have a highly viscous annulus of fluid surrounding a much less viscous core. In this case, we non-dimensionalize using the more viscous fluid: $\mathscr{V} = \sigma_2/\mu_1$. We also redefine the Reynolds number so that it is scaled upon μ_1: $Re_1 = \rho_1 \mathscr{V} R/\mu_1$. The non-dimensional governing equations in the annular region are then given by

$$Re_1\left(u_{1_t} + u_1 u_{1_r} + w_1 u_{1_z}\right) = -p_{1_r} + \left(\frac{1}{r}[r u_{1_r}]_r - \frac{u_1}{r^2} + \epsilon^2 u_{1_{zz}}\right), \tag{2.40}$$

$$Re_1\left(w_{1_t} + u_1 w_{1_r} + w_1 w_{1_z}\right) = -\epsilon^2 p_{1_z} + \left(\frac{1}{r}[r w_{1_r}]_r + \epsilon^2 w_{1_{zz}}\right), \tag{2.41}$$

$$\frac{1}{r}(r u_1)_r + w_{1_z} = 0. \tag{2.42}$$

In the core region, we have

$$\frac{m}{l}Re_1\left(u_{2_t}+u_2u_{2_r}+w_2u_{2_z}\right)=-mp_{2_r}+\left(\frac{1}{r}[ru_{2_r}]_r-\frac{u_2}{r^2}+\epsilon^2u_{2_{zz}}\right), \tag{2.43}$$

$$\frac{m}{l}Re_1\left(w_{2_t}+u_2w_{2_r}+w_2w_{2_z}\right)=-\epsilon^2mp_{2_z}+\left(\frac{1}{r}[rw_{2_r}]_r+\epsilon^2w_{2_{zz}}\right), \tag{2.44}$$

$$\frac{1}{r}(ru_2)_r+w_{2_z}=0. \tag{2.45}$$

The normal and shear stress balances at $r=S_1$ are, respectively, given by

$$p_1-\frac{2}{1+\epsilon^2S_{1_z}^2}\left(u_{1_r}-S_{1_z}\left[\epsilon^2u_{1_z}+w_{1_r}\right]+\epsilon^2S_{1_z}^2w_{1_z}\right)=\gamma\left(\frac{1}{S_1}-\epsilon^2S_{1_{zz}}\right), \tag{2.46}$$

$$\left(1-\epsilon^2S_{1_z}^2\right)\left(w_{1_r}+\epsilon^2u_{1_z}\right)+2\epsilon^2S_{1_z}\left(u_{1_r}-w_{1_z}\right)=0. \tag{2.47}$$

The equivalent balances at $r=S_2$ are given by

$$p_2-\frac{2}{m\left(1+\epsilon^2S_{2_z}^2\right)}\left(\epsilon^2S_{2_z}^2w_{2_z}-S_{2_z}\left(\epsilon^2u_{2_z}+w_{2_r}\right)+u_{2_r}\right)$$
$$-\left(p_1-\frac{2}{\left(1+\epsilon^2S_{2_z}^2\right)}\left(\epsilon^2S_{2_z}^2w_{1_z}-S_{2_z}\left(\epsilon^2u_{1_z}+w_{1_r}\right)+u_{1_r}\right)\right)=\left(\frac{1}{S_2}-\epsilon^2S_{2_{zz}}\right), \tag{2.48}$$

$$\left[\left(1-\epsilon^2S_{2_z}^2\right)\left(\epsilon^2u_{2_z}+w_{2_r}\right)+2\epsilon^2S_{2_z}\left(u_{2_r}-w_{2_z}\right)\right]$$
$$-m\left[\left(1-\epsilon^2S_{2_z}^2\right)\left(\epsilon^2u_{1_z}+w_{1_r}\right)+2\epsilon^2S_{2_z}\left(u_{1_r}-w_{1_z}\right)\right]=0. \tag{2.49}$$

2.2.1. *Asymptotic reduction*

We consider the distinguished limits $m=M/\epsilon^2$, $l=L/\epsilon^2$ and $Re=\epsilon^2\overline{Re}$ in the above equations. This canonical limit is chosen to retain inertia in the leading-order equations. Once again, the comments made in § 2.1.1 regarding the magnitude of the density ratio are equally applicable to this case. The Stokes limit and the way it can be achieved asymptotically is discussed at the end of this section. From the leading-order axial component of the Navier–Stokes equations in the annular region and the shear stress balance at $r=S_1$, which are, respectively, given by

$$\frac{1}{r}[rw_{1_r}]_r=0, \quad w_{1_r}=0, \tag{2.50}$$

we find that the leading-order annular axial velocity $w_1\equiv w_1(z,t)$, that is, it is independent of the radial coordinate. Substitution of this result into the leading-order normal stress balance at $r=S_1$ and the continuity equation yields the following

$$p_1=\gamma\left(\frac{1}{S_1}-\epsilon^2S_{1_{zz}}\right)+2u_{1_r}(S_1,z,t), \quad u_1=-w_{1_z}\frac{r}{2}+\frac{a_1(z,t)}{r}. \tag{2.51}$$

From the leading-order axial component of the Navier–Stokes equations in the core given by

$$Mp_{2_z}=\frac{1}{r}[rw_{2_r}]_r, \tag{2.52}$$

and using the fact that $p_{1_r}=0$ to leading order from the radial momentum equation, we obtain

$$w_2=\tfrac{1}{4}Mr^2p_{2_z}-a_2(z,t). \tag{2.53}$$

Substitution of w_2 into the continuity equation yields

$$u_2 = -\left(M\frac{r^3}{16}p_{2_{zz}} - \frac{r}{2}a_{2_z}\right); \tag{2.54}$$

where we have used boundedness at $r = 0$. From the leading-order normal stress balance at $r = S_2$, we obtain

$$p_2 = p_1 + \left(\frac{1}{S_2} - \epsilon^2 S_{2_{zz}}\right) - 2u_{1_r}(S_2, z, t). \tag{2.55}$$

Demanding continuity of axial and radial velocities at $r = S_2$ leads to

$$a_2(z, t) = M\frac{S_2^2}{4}p_{2_z} - w_1, \tag{2.56}$$

$$\begin{aligned} a_1(z, t) &= -\tfrac{1}{16}MS_2^4 p_{2_{zz}} + \tfrac{1}{2}S_2^2 a_{2_z} + \tfrac{1}{2}S_2^2 w_{1_z} \\ &= -\left(\tfrac{1}{16}MS_2^4 p_{2_{zz}} - \tfrac{1}{2}S_2^2\left(\tfrac{1}{4}M\left(S_2^2 p_{2_z}\right)_z - w_{1_z}\right)\right) + \tfrac{1}{2}S_2^2 w_{1_z}. \end{aligned} \tag{2.57}$$

In order to generate an evolution equation for w_1 we consider the second-order axial component of the Navier–Stokes equations in the annular region:

$$\overline{Re}\left(w_{1_t} + w_1 w_{1_z}\right) = -p_{1_z} + \left(w_{1_{zz}} + \frac{1}{r}\left[r w_{1_r}^{(2)}\right]_r\right), \tag{2.58}$$

in which $w_1^{(2)}$ represents the second-order contribution to the axial velocity component in the annular region. Integration of this equation yields

$$\tfrac{1}{2}r\left(\overline{Re}\left(w_{1_t} + w_1 w_{1_z}\right) + \left(p_{1_z} - w_{1_{zz}}\right)\right) = w_{1_r}^{(2)} + \frac{a_3(z, t)}{r}. \tag{2.59}$$

Substitution of $w_{1_r}^{(2)}$ into the second-order shear stress balance at $r = S_1$, given by

$$w_{1_r}^{(2)} + u_{1_z} + 2S_{1_z}\left(u_{1_r} - w_{1_z}\right) = 0, \tag{2.60}$$

yields an equation for $a_3(z, t)$:

$$\begin{aligned} a_3(z, t) = {} & \tfrac{1}{2}S_1^2\left(\overline{Re}\left(w_{1_t} + w_1 w_{1_z}\right) + \left(p_{1_z} - w_{1_{zz}}\right)\right) \\ & - \tfrac{1}{2}S_1^2 w_{1_{zz}} + a_{1_z} - 2\frac{S_{1_z}}{S_1}a_1 - 3S_1 S_{1_z} w_{1_z}. \end{aligned} \tag{2.61}$$

Another equation for $a_3(z, t)$ can be obtained by substituting $w_{1_r}^{(2)}$ into the second-order shear stress balance at $r = S_2$, given by

$$\frac{1}{M}w_{2_r} - \left(u_{1_z} + 2S_{2_z}\left(u_{1_r} - w_{1_z}\right)\right) = w_{1_r}^{(2)}; \tag{2.62}$$

this, then, yields

$$\begin{aligned} a_3(z, t) = {} & \tfrac{1}{2}S_2^2\left(\overline{Re}\left(w_{1_t} + w_1 w_{1_z}\right) + \left(p_{1_z} - w_{1_{zz}}\right)\right) \\ & - \frac{S_2}{M}w_{2_r}(S_2, z, t) + S_2\left(u_{1_z} + 2S_{2_z}\left(u_{1_r} - w_{1_z}\right)\right)(S_2, z, t). \end{aligned} \tag{2.63}$$

By equating (2.61) and (2.63), an evolution equation for w_1 is obtained:

$$\begin{aligned} \left(\overline{Re}\left(w_{1_t} + w_1 w_{1_z}\right) + p_{1_z} - w_{1_{zz}}\right)\tfrac{1}{2}\left(S_1^2 - S_2^2\right) - \tfrac{1}{2}\left(S_1^2 - S_2^2\right)w_{1_{zz}} - \tfrac{3}{2}\left(S_1^2 - S_2^2\right)_z w_{1_z} \\ - \tfrac{1}{2}S_2^2 p_{2_z} - 2\left(\frac{S_{1_z}}{S_1} - \frac{S_{2_z}}{S_2}\right)a_1 = 0, \end{aligned} \tag{2.64}$$

where κ_1 is given by (2.16).

Substitution of (2.51) into (2.55) yields

$$p_2 = \gamma\kappa_1 + \kappa_2 + 2a_1\left(\frac{1}{S_2^2} - \frac{1}{S_1^2}\right), \tag{2.65}$$

from which a_1 can be eliminated:

$$a_1(z,t) = S_1^2 S_2^2 \frac{[p_2 - (\gamma\kappa_1 + \kappa_2)]}{2\left(S_1^2 - S_2^2\right)}. \tag{2.66}$$

Elimination of p_1 and a_1 from (2.64) yields

$$\overline{Re}\left(w_{1_t} + w_1 w_{1_z}\right)\left(S_1^2 - S_2^2\right) - 3\left[\left(S_1^2 - S_2^2\right) w_{1_z}\right]_z + \gamma S_1^2(\kappa_1)_z + S_2^2(\kappa_2)_z = 0. \tag{2.67}$$

An equation for p_2 is obtained by equating (2.57) and (2.66):

$$p_2 - (\gamma\kappa_1 + \kappa_2) + \tfrac{1}{8}M\left[1 - \left(\frac{S_2}{S_1}\right)^2\right]\left[S_2^2 p_{2_{zz}} - 2\left(S_2^2 p_{2_z}\right)_z\right] = 0. \tag{2.68}$$

Equation (2.68) provides the leading-order pressure in the core and couples into the following evolution equations for S_1, and S_2:

$$S_{1_t} + w_1 S_{1_z} + \tfrac{1}{2}S_1 w_{1_z} = 0, \tag{2.69}$$

$$S_{2_t} + w_1 S_{2_z} + \tfrac{1}{2}S_2 w_{1_z} = \tfrac{1}{16}M\left(S_2^4 p_{2_z}\right)_z \frac{1}{S_2}. \tag{2.70}$$

It is easy to see that (2.69)–(2.70) conserve the integrals of S_1^2 and S_2^2, respectively, which physically corresponds to mass conservation. Before we consider the linear stability of the system, we discuss the Stokes limit.

The distinguished limits $m \sim \epsilon^{-2}$, $l \sim \epsilon^{-2}$, $Re_1 \sim \epsilon^2$, were chosen to provide inertia in the leading-order evolution. Inertia enters through the second-order contribution to the axial velocity in the z-momentum equation (2.2). It can be seen, therefore, that if

$$Re_1 \ll \frac{m}{l}Re_1 \sim \frac{Re_1}{\epsilon^2 l}, \tag{2.71}$$

holds, then inertia is unimportant in the annulus at second order. If we also have $Re_1/l \ll 1$, then the asymptotic balances in the core region remain valid to the order carried out (this last inequality essentially permits the balance of viscous terms with the axial pressure gradient in the core, to leading order, with the solution (2.53) emerging). It is worth noting that this limit is valid for $l = O(1)$ also. The resulting evolution equations in the Stokes limit are (2.67), (2.68) and (2.69)–(2.70), with $\overline{Re}_1 \equiv 0$. We note further that in the case where κ_1 and κ_2 consist of ϵ^0 terms alone, (2.67) can be integrated in z to give

$$3\left(S_1^2 - S_2^2\right)w_{1_z} + \gamma S_1 + S_2 = f(t), \tag{2.72}$$

where $f(t)$ corresponds to the quasi one-dimensional force in the jet (see Renardy 1994; Papageorgiou 1995*a*, *b*). We will not study the Stokes problem further in this work. Once again, we can remove the Reynolds number explicitly from the equations by performing the rescaling in (2.30) (using $\overline{Re}_1$) supplemented with

$$p_2 \to p_2/\overline{Re}_1, \quad M \to M/\overline{Re}_1^2.$$

2.2.2. *Connections with previous models*

We can establish connections between (2.67), (2.68), (2.69) and (2.70) and other models in the literature. In the limit $M \to 0$, the equations studied in paper I are again recovered. The lubrication equations governing the dynamics of a thin core surrounded by a much more viscous liquid of infinite extent, which was studied by Sierou & Lister (2003) can also be recovered. To this end, we set $\epsilon = 0$ and take $S_1 \gg S_2$ in (2.72), which yields $w_{1_z} \approx 0$. Since $w_1 \to 0$ as $r \to \infty$, $w_1 = 0$. As a result, (2.70) becomes

$$S_2 S_{2_t} \approx \tfrac{1}{16} M \left(S_2^4 p_{2_z}\right)_z. \tag{2.73}$$

Taking $S_1 \gg S_2$ in (2.68) yields

$$p_2 \approx \frac{1}{S_2} + \tfrac{1}{8} M \left(2\left(S_2^2 p_{2_z}\right)_z - S_2^2 p_{2_{zz}}\right), \tag{2.74}$$

which, using (2.73) yields

$$p_2 \approx \frac{1}{S_2} + 2\frac{S_{2_t}}{S_2}. \tag{2.75}$$

Equations (2.73) and (2.75) are the dimensionless analogues of (4.3) and (4.5) in the work of Sierou & Lister (2003).

3. Linear theory

We now conduct a linear stability analysis of the equations governing the dynamics of the highly viscous core and annulus to determine the band of unstable wavenumbers for a given set of parameters. The results of this section will also be used in order to validate the numerical results near the onset of the instability and aid in our interpretation.

3.1. *Highly viscous core*

We investigate the linear stability characteristics of the governing equations (2.27)–(2.29) (after scaling $\overline{Re}$ out) that govern the initial dynamics of a highly viscous fluid core surrounded by a much less viscous fluid annulus. The ratio of undisturbed outer to inner interface positions is denoted by α. We insert the following decomposition into these equations

$$(S_1,\ S_2,\ w_2) = (\alpha,\ 1,\ 0) + (\tilde{S}_1,\ \tilde{S}_2,\ \tilde{w}_2), \tag{3.1}$$

where the quantities with tildes correspond to infinitesimal perturbation. Subsequent linearization of (2.27) and (2.29) then yields

$$\tilde{S}_{1_t} = \tilde{u}_1|_\alpha, \quad \tilde{S}_{2_t} = -\tfrac{1}{2}\tilde{w}_{2_z}, \tag{3.2}$$

$$\tilde{w}_{2_t} = 3\tilde{w}_{2_{zz}} + \left(\tilde{S}_{2_z} + \epsilon^2 \tilde{S}_{2_{zzz}}\right) + \gamma\left(\tilde{S}_{1_z} + \epsilon^2\alpha^2 \tilde{S}_{1_{zzz}}\right), \tag{3.3}$$

in which $\tilde{u}_1$ is given by

$$\tilde{u}_1|_\alpha = -\tfrac{1}{2}\alpha\tilde{w}_{2_z} - \frac{\gamma A}{\alpha^2}\left(\tilde{S}_{1_{zz}} + \epsilon^2\alpha^2\tilde{S}_{1_{zzzz}}\right). \tag{3.4}$$

Here, $A \equiv [\alpha - (3\alpha^3/4) - (1/4\alpha) + \alpha^3 \ln\alpha]/(4M)$. Substitution of a normal mode expansion into (3.2) and (3.3) of the form

$$(\tilde{S}_1, \tilde{S}_2, \tilde{w}) = (\hat{S}_1, \hat{S}_2, \hat{w})\mathrm{e}^{\mathrm{i}kz}\mathrm{e}^{\lambda t}, \tag{3.5}$$

in which λ and k represent the complex perturbation growth rate and real wavenumber, respectively, leads to the following characteristic equation for λ

$$[2\lambda(\lambda + 3k^2) - k^2(1 - \epsilon^2 k^2)]\left(\lambda - \frac{\gamma A}{\alpha^2}k^2[1 - \epsilon^2\alpha^2 k^2]\right) = \lambda\alpha\gamma k^2(1 - \epsilon^2\alpha^2 k^2). \quad (3.6)$$

This equation admits cutoff modes, which are given by $k_c = 1/\epsilon$ and $k_c = 1/(\epsilon\alpha)$; these have physical interpretations as the two interfaces can each release energy via the Rayleigh mechanism and these cutoffs emerge from this.

In the limit of small k, we find that λ can be approximated by either $\lambda \sim \lambda_1 k$ or $\lambda \sim \lambda_2 k^2$:

$$\lambda \sim \pm\left(\frac{1 + \alpha\gamma}{2}\right)^{1/2} k, \quad (3.7)$$

$$\lambda \sim \frac{\gamma A}{\alpha^2(1 + \alpha\gamma)}k^2. \quad (3.8)$$

These small k results are consistent with the equivalent limit in the full linear stability problem of a viscous compound thread studied by Chauhan *et al.* (2000), and in particular their long-wave limit expressions, (23) and (24), for the growth rates of the stretching and squeezing modes, respectively. The former growth rates are identical to (3.7) when the density ratio d of Chauhan *et al.* (2000) is set to zero, and the squeezing growth rate (24) is identical to (3.8) on setting $m \sim \epsilon^2$ and expressing it in terms of our non-dimensionalization.

In order to determine whether any potentially unstable modes correspond to 'stretching' or 'squeezing' modes, which evolve in-phase or out-of-phase, respectively, we form the ratio of $\hat{S}_1$ to $\hat{S}_2$:

$$\frac{\hat{S}_1}{\hat{S}_2} = \frac{\alpha^3}{\lambda\alpha^2 - \gamma A k^2(1 - \epsilon^2\alpha^2 k^2)}\frac{1}{\lambda}. \quad (3.9)$$

Stretching and squeezing modes correspond to positive and negative values of $\hat{S}_1/\hat{S}_2$, respectively. In the small k limit and assuming that $\lambda \sim \lambda_1 k$, (3.9) becomes

$$\frac{\hat{S}_1}{\hat{S}_2} \sim \frac{2\alpha}{k^2(1 + \alpha\gamma)} > 0. \quad (3.10)$$

Inspection of these equations suggests that the mode associated with the asymptotic behaviour given by (3.7) corresponds to a stretching mode. Assuming that $\lambda \sim \lambda_2 k^2$, (3.9) becomes

$$\frac{\hat{S}_1}{\hat{S}_2} \sim -\frac{\alpha^4(1 + \alpha\gamma)^2}{A^2\gamma^3 k^4} < 0, \quad (3.11)$$

from which it is evident that this mode corresponds to a squeezing mode. The ratio of the two modes in the small k limit is given by

$$\frac{\lambda_1 k}{\lambda_2 k^2} \sim \frac{\alpha^2(1 + \alpha\gamma)^{3/2}}{2^{1/2}\gamma A k}, \quad (3.12)$$

which indicates that the stretching mode dominates in this limit. Careful inspection of this equation further reveals that this ratio scales as $\alpha^{1/2}/\ln\alpha$ for $\alpha \gg 1$ and diverges as $\alpha \to 1$, implying that the stretching mode remains dominant for both small and large α values. Moreover, this ratio scales as $\gamma^{1/2}$ and γ^{-1} for large and small γ, implying that the stretching mode is also dominant over the squeezing mode

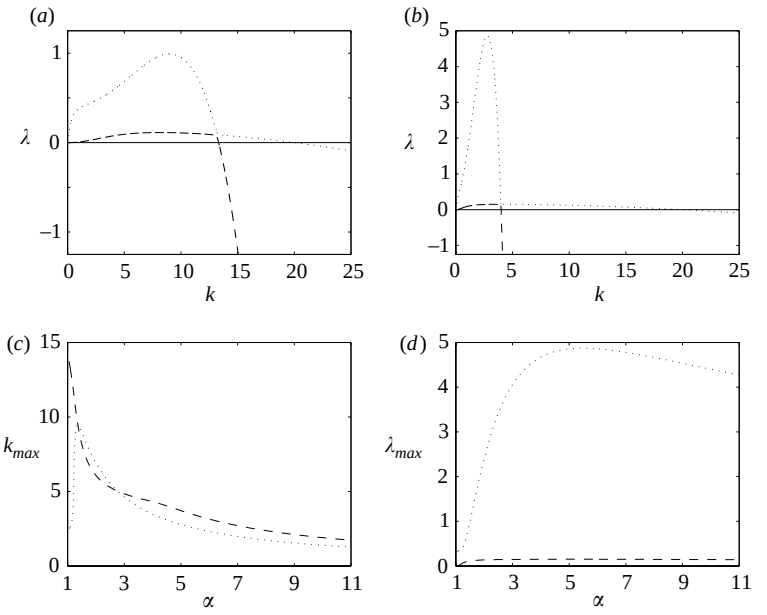

FIGURE 2. Effect of α on the linear stability characteristics when the core is more viscous than the annulus. Dispersion curves with $\alpha = 1.5$ and 5, shown in (a) and (b), respectively, $M = \gamma = 1$ and $\epsilon = 0.05$ showing two modes: a stretching mode (dotted line), which is dominant over all k values, a squeezing mode (dashed line), which is unstable over $0 \leqslant k \leqslant 1/(\epsilon\alpha)$. Another squeezing mode, not shown, is stable for all k. The wavenumber of the most dangerous mode and the associated maximal growth rates are shown in (c) and (d), respectively, for the same parameter values as in (a) and (b).

in the limit of small k for both small and large γ. Furthermore, since $A > 0$ for $\alpha > 1$, then in the range $0 \leqslant k \leqslant 1/(\alpha\epsilon)$ an unstable mode with $\lambda > 0$ is a stretching mode if $\lambda > (\gamma A k^2)(1 - \epsilon^2\alpha^2k^2)/\alpha^2$, otherwise it is a squeezing mode. In the range $(1/\alpha\epsilon) < k < 1/\epsilon$, $\gamma A k^2(1 - \epsilon^2\alpha^2k^2) < 0$. Thus if $\lambda > 0$, then the associated mode is a stretching mode.

Typical dispersion curves are shown in figure 2. Inspection of figures 2(a) and 2(b) reveals that there exist three modes: a stretching mode (dotted line), which is dominant over all k values and unstable over $0 \leqslant k \leqslant 1/\epsilon$; a squeezing mode (dashed line), which is unstable over $0 \leqslant k \leqslant 1/(\epsilon\alpha)$; and another squeezing mode (not shown) stable for all k. These dispersion curves are single-humped and have a well-defined most dangerous mode at an intermediate value of k, k_{max}, for which λ is λ_{max}. Although the band of unstable wavenumbers of the stretching mode, $0 < k < k_c = 1/\epsilon$, remains unaltered, the analogous band for the squeezing mode, $0 \leqslant k \leqslant 1/(\epsilon\alpha)$ becomes narrower; the growth rate associated with the stretching mode increases and so it increases in dominance with increasing α, which corresponds to a relative decrease in the thickness of the core.

From figures 2(c) and 2(d), it is clear that there exists an intermediate value of α which maximizes the value of the wavenumber associated with the most dangerous mode k_{max} of the stretching mode as well as the maximal growth rates of both modes, λ_{max}, although λ_{max} associated with the stretching mode appears to be more sensitive to variations in α than the squeezing mode. Thus for α values larger or smaller than approximately $\alpha \approx 1.5$ for the parameters used to generate figure 2, we expect to see

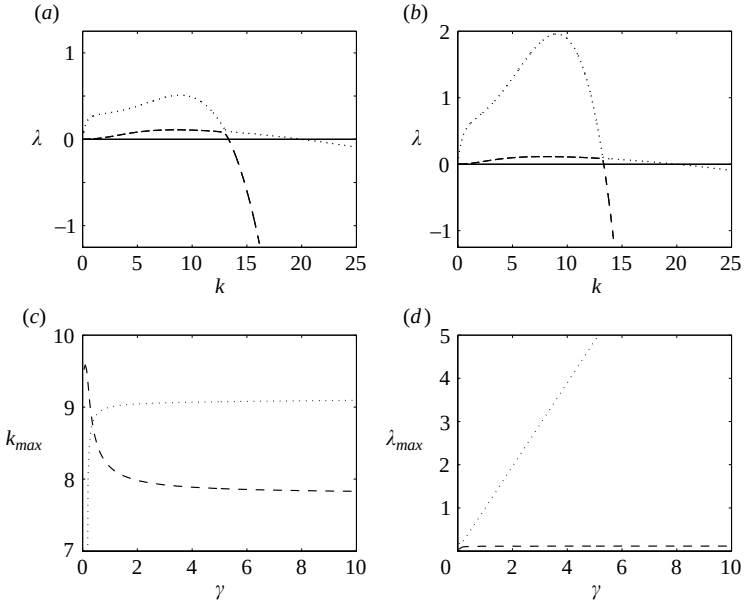

FIGURE 3. Effect of γ on the linear stability characteristics when the core is more viscous than the annulus. Dispersion curves generated with $\gamma = 0.5$ and 2 are shown in (a) and (b), respectively, $\alpha = 1.5$, $M = 1$ and $\epsilon = 0.05$, showing the same two modes as those shown in figure 2. The wavenumber of the most dangerous mode and the associated growth rates are shown in (c) and (d), respectively for the same parameters as in (a) and (b).

increasingly larger structures. These results may appear to be somewhat unexpected since one would have anticipated that an increase in α, or a reduction in the relative thickness of the highly viscous core should result in a sufficient reduction in viscous dissipation so as to increase the magnitude of both k_{max} and λ_{max} monotonically. These results, however, can be explained by recalling first that r was scaled on $\mathscr{R}$, the radius of the core, which implies that the pressure (viscous resistance) associated with the outer interface decreases (increases) with α. In the case of the squeezing mode, the flow is increasingly driven by the inner interface with increasing α, thus the maximal growth rate becomes essentially independent of α for sufficiently large α values. The decrease in k_{max} with α may be attributed to the increase in relative significance of the resistance to extensional flow within the core to the resistance to lubrication flow in the annular region.

We have also investigated the effect of varying γ, the surface tension ratio, on the linear stability characteristics of the threads, which is shown in figure 3. As shown in figures 3(a) and 3(b), increasing γ increases the relative dominance of the stretching mode over the squeezing mode, while leaving the wavenumbers associated with the cutoff and most dangerous modes unaltered for $\gamma > 2$. This is confirmed upon inspection of figures 3(c) and 3(d) which show the effect of varying γ on k_{max} and λ_{max}, respectively. Figure 3(d) indicates that increasing the relative magnitude of the outer interfacial tension has a particularly destabilizing influence on the stretching mode, leaving the squeezing mode comparatively unchanged. Thus, we may tentatively conclude that the presence of surfactant at the inner interface, which lowers the mean value of the interfacial tension there, will lead to more rapid breakup and may not necessarily alter the size of the structures formed. This prediction, however, does not

take into account the presence of surfactant-induced Marangoni stresses, which act to rigidify the interface and, depending on its concentration and its 'strength' may drastically alter the transient dynamics (paper I; Craster *et al.* 2002). Note also that variation of either α or γ does not result in cross-over of the λ_{max} curves of the two modes, implying that one cannot enforce the dominant mode via simple variation of these parameters in the linear regime.

Finally, the asymptotic formula for the growth rate in the small m and l limits is given by (see paper I)

$$\lambda \sim \tfrac{1}{2}(-3k^2 \pm \sqrt{9k^4 + 2(1+\alpha\gamma - \epsilon^2(\alpha^3\gamma+1)k^2)}), \tag{3.13}$$

which agrees with that obtained from (3.6) in the limit $M \to \infty$.

Thus the results presented here indicate that, in contrast to the work presented in paper I, there exist two unstable modes rather than one and that the stretching mode is dominant over the squeezing mode for all relevant parameter values; this is in agreement with the results of Chauhan *et al.* (2000*b*) who find that the stretching mode is the most dominant for all parameter values considered in their extensive study. Hence, despite the fact that the predictions of linear theory are only valid near onset, we may expect the stretching mode to persist and the two interfaces to grow in phase in the nonlinear regime. In order to quantify this linear result, we solve the nonlinear evolution starting with small-amplitude initial conditions, thus allowing the system to select the most unstable mode and evolve it into the nonlinear regime and possibly breakup.

3.2. *Highly viscous annulus*

Here, we follow a similar approach to that employed in the viscous core case. We linearize (2.64), (2.68) and (2.70) (after scaling $\overline{Re}$ out) using the following normal mode expansion:

$$(S_1,\ S_2,\ w_1,\ p_2) = (\alpha,\ 1,\ 0,\ 1+\gamma/\alpha) + (\hat{S}_1,\ \hat{S}_2,\ \hat{w},\ \hat{p})\mathrm{e}^{\mathrm{i}kz}\mathrm{e}^{\lambda t}, \tag{3.14}$$

which gives rise to the following equations for the disturbance quantities:

$$\lambda\hat{S}_1 + \tfrac{1}{2}\mathrm{i}\alpha k\hat{w} = 0, \tag{3.15}$$

$$\lambda\hat{S}_2 + \frac{M}{2}\left(\frac{\mathrm{i}}{M}k\hat{w} + \frac{k^2}{8}\hat{p}\right) = 0, \tag{3.16}$$

$$(\alpha^2-1)(\lambda+3k^2)\hat{w} - \mathrm{i}k\gamma(1-\epsilon^2\alpha^2k^2)\hat{S}_1 - \mathrm{i}k(1-\epsilon^2k^2)\hat{S}_2 = 0, \tag{3.17}$$

$$\left(1 + \frac{k^2M}{8\alpha^2}[\alpha^2-1]\right)\hat{p} + \frac{\gamma}{\alpha^2}(1-\epsilon^2\alpha^2k^2)\hat{S}_1 + (1-\epsilon^2k^2)\hat{S}_2 = 0. \tag{3.18}$$

Manipulation of (3.15)–(3.18) yields the following characteristic equation for λ:

$$(\alpha^2-1)(\lambda+3k^2) - \frac{k^2\alpha\gamma}{2\lambda}(1-\epsilon^2\alpha^2k^2) - \frac{Mk^2}{2\lambda}(1-\epsilon^2k^2)\left[\frac{1}{M} + \frac{k^2}{8}\left(\frac{\dfrac{\gamma(1-\epsilon^2\alpha^2k^2)}{\alpha} + (1-\epsilon^2k^2)}{1+\left(B - \dfrac{M}{16\lambda}(1-\epsilon^2k^2)\right)k^2}\right)\right] = 0, \tag{3.19}$$

in which $B = (\alpha^2-1)M/(8\alpha^2)$. This equation also admits cutoff modes, k_c, given by $k_c = 1/\epsilon$ and $k_c = 1/(\epsilon\alpha)$.

The ratio of $\hat{S}_2$ to $\hat{S}_1$ is given by

$$\frac{\hat{S}_2}{\hat{S}_1} = \frac{1}{\alpha} + \frac{Mk^2[(1-\epsilon^2k^2)+\gamma(1-\epsilon^2\alpha^2k^2)/\alpha]}{16\alpha\lambda(1+k^2[B-M(1-\epsilon^2k^2)/16\lambda])}. \tag{3.20}$$

In the limit of small k, λ can, once again, be approximated by $\lambda \sim \lambda_1 k$ or $\lambda \sim \lambda_2 k^2$, where λ_1 and λ_2 are expressed by

$$\lambda_1 = \pm\left(\frac{\alpha\gamma+1}{2(\alpha^2-1)}\right)^{1/2}, \tag{3.21}$$

$$\lambda_2 = \frac{\gamma M(\alpha^2-1)}{16\alpha(\alpha\gamma+1)}. \tag{3.22}$$

Thus for $k \ll 1$ and $\lambda = \lambda_1 k$, (3.20) becomes

$$\frac{\hat{S}_2}{\hat{S}_1} \sim \frac{1}{\alpha}, \tag{3.23}$$

indicating that this mode corresponds to a stretching mode. For $\lambda = \lambda_2 k^2$, (3.20) becomes

$$\frac{\hat{S}_2}{\hat{S}_1} \sim \frac{1-\alpha(\alpha\gamma+1)}{\alpha}, \tag{3.24}$$

which is negative for all values of α and γ indicating that this is a squeezing mode.

It also proves instructive to examine the ratio of the growth rates associated with each mode in the small k limit:

$$\frac{\lambda_1 k}{\lambda_2 k^2} = \frac{16\alpha}{2^{1/2}\gamma M k}\left(\frac{\alpha\gamma+1}{\alpha^2-1}\right)^{3/2}. \tag{3.25}$$

This ratio is, as $\alpha \to \infty$, proportional to $\alpha^{-1/2}$ and diverges in the limit $\alpha \to 1$. This indicates that the stretching mode is less (more) dominant in the former (latter) limit for small k. Similarly, this ratio scales as $\gamma^{1/2}$ and γ^{-1} in the large and small γ limits, respectively, indicating that the stretching mode always dominates.

In figures 4(a) and 4(b), we show the effect of varying α on the dispersion curves for the highly viscous annulus case. There exist, once again, three distinct modes: a stretching mode (dotted line), which is unstable over the range $0 \leqslant k \leqslant 1/\epsilon$ and dominant over all k values, a squeezing mode (dashed line), which is unstable over $0 \leqslant k \leqslant 1/(\epsilon\alpha)$ and another squeezing mode (not shown), stable for all k. The dispersion curves in this case are also single-humped with a well-defined most dangerous mode associated with an intermediate k value, k_{max}, for which the growth is maximal, λ_{max}. In contrast to the highly viscous core case, variation of α in this case does not give rise to maxima in λ_{max}. As shown in figures 4(a) and 4(b), k_{max} rises sharply for both the stretching and squeezing modes as $\alpha \to 1$, as does λ_{max} of the stretching mode; the latter can be explained upon inspection of (3.21), which diverges as α approaches unity. Increasing α results in a sharp decrease of k_{max} and λ_{max} of the stretching mode, which then saturate beyond a value of $\alpha \approx 2$ for this set of parameter values; in fact, k_{max} exhibits a very shallow minimum with respect to α (see figure 4c). The analogous quantities for the squeezing mode, on the other hand, decrease monotonically with increasing α. Thus it appears that decreasing the relative thickness of the highly viscous annulus, which effectively decreases the magnitude of viscous dissipation has a particularly destabilizing influence on the system.

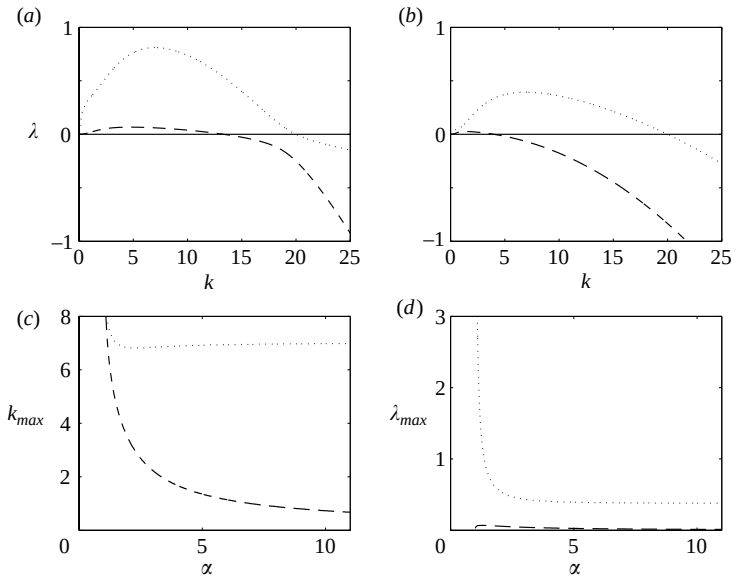

FIGURE 4. Effect of α on the linear stability characteristics when the core is less viscous than the annulus. Dispersion curves generated with $\alpha = 1.5$ and 5 are shown in (*a*) and (*b*), respectively, $M = \gamma = 1$ and $\epsilon = 0.05$ showing two modes: a stretching mode (dotted line), which is dominant over all k values and unstable for $0 \leqslant k \leqslant 1/\epsilon$, a squeezing mode (dash line), which is unstable over $0 \leqslant k \leqslant 1/(\epsilon\alpha)$. There is another squeezing mode (not shown) that is stable for all k. The wavenumber of the most dangerous mode and the associated growth rates are shown in (*c*) and (*d*), respectively, for the same parameters as in (*a*) and (*b*).

Variation of γ (see figure 5) has a similar effect on the linear stability of the highly viscous annulus case as that previously demonstrated for the viscous core case. In particular, increasing γ increases the relative dominance of the stretching mode, although in this case k_{max} and λ_{max} of both modes appear to be sensitive to changes in γ.

We have also checked that the limiting formula in the limit $M \to 0$ expressed by

$$\lambda \sim \frac{-3(\alpha^2-1)k^2 \pm \sqrt{[3(\alpha^2-1)k^2]^2 + 2(\alpha^2-1)k^2(\alpha\gamma + 1 - \epsilon^2 k^2[\alpha^3\gamma + 1])}}{2(\alpha^2-1)}, \quad (3.26)$$

is in agreement with the limiting formula for λ in the large m and l limits (see paper I).

The predictions made here are largely similar to those for highly viscous cores: the stretching mode dominates the squeezing mode and the interfaces will initially grow in phase. The ultimate interfacial shapes near pinchoff may be complicated and can only be predicted via numerical simulations of the evolution equations. A discussion of these simulations is presented in the following section.

4. Numerical simulations

We begin the presentation of the numerical results with a brief description of the numerical procedure. The evolution equations, (2.27) and (2.29), are solved using a pseudo-spectral code that uses fast Fourier transform (FFT) methods for the spatial derivatives (typically 512 modes, doubling or halving the number of modes made no discernible difference to the computations) and Gear's method to advance the solution in time from the prescribed initial conditions. These are chosen to be either

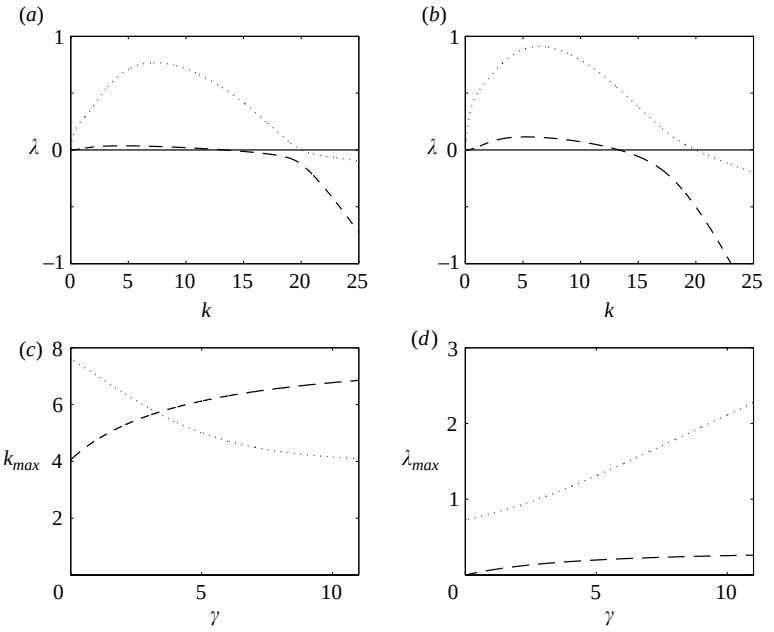

FIGURE 5. Effect of γ on the linear stability characteristics when the core is less viscous than the annulus. Dispersion curves generated with $\gamma = 0.5$ and 2 shown in (a) and (b), respectively, $\alpha = 1.5$, $M = 1$ and $\epsilon = 0.05$, showing the same two modes as those shown in figure 4. The wavenumber of the most dangerous mode and the associated growth rates are shown in (c) and (d), respectively for the same parameters as in (a) and (b).

random perturbations of initially small amplitude, taken from a uniform distribution on $10^{-5}[-1, 1]$, or the dominant mode from linear theory. In the latter case, we take an initial condition from (3.1), (3.5) with $\hat{S}_1 = 10^{-4}$ (the other perturbations are found from this) and $\lambda(k)$ from (3.6). This has the advantage that we can track linear theory and verify the predictions of the numerical procedure; clearly since the code is Fourier spectral in origin, periodic boundary conditions are applied.

The length of the computational domain is chosen to be from -10 to 10 for random initial conditions and $4\pi/k$ for those started with the most dangerous mode (twice the wavelength of the most dangerous mode to allow nonlinear evolution to longer structures if the equations so desire). The computations are halted immediately before the dimensionless distance between S_1 and S_2 is of order 10^{-4}, or when $S_2 \sim O(10^{-4})$.

4.1. *Highly viscous core*

The results of our simulations for typical parameter values are shown in figure 6. Here we show the effect of varying the initial thickness ratio on the dynamics for $\alpha = 1.5, 5, 10$ and $\gamma = 1$. The compound thread evolution is initiated as described above; the results associated with the pseudo-random initial conditions are shown in the left-hand panels, while those starting from the most dangerous mode are depicted in the right-hand panels.

In both cases, the thread evolves under the action of capillarity, which acts to amplify the initially small disturbances. The highly viscous core forms a varicose, gently varying, interior surrounded by a rapidly varying outer less viscous annulus. Clearly, the less viscous annulus is more susceptible to deformations than the core. The behaviour shown in figure 6 is markedly different from that presented in paper

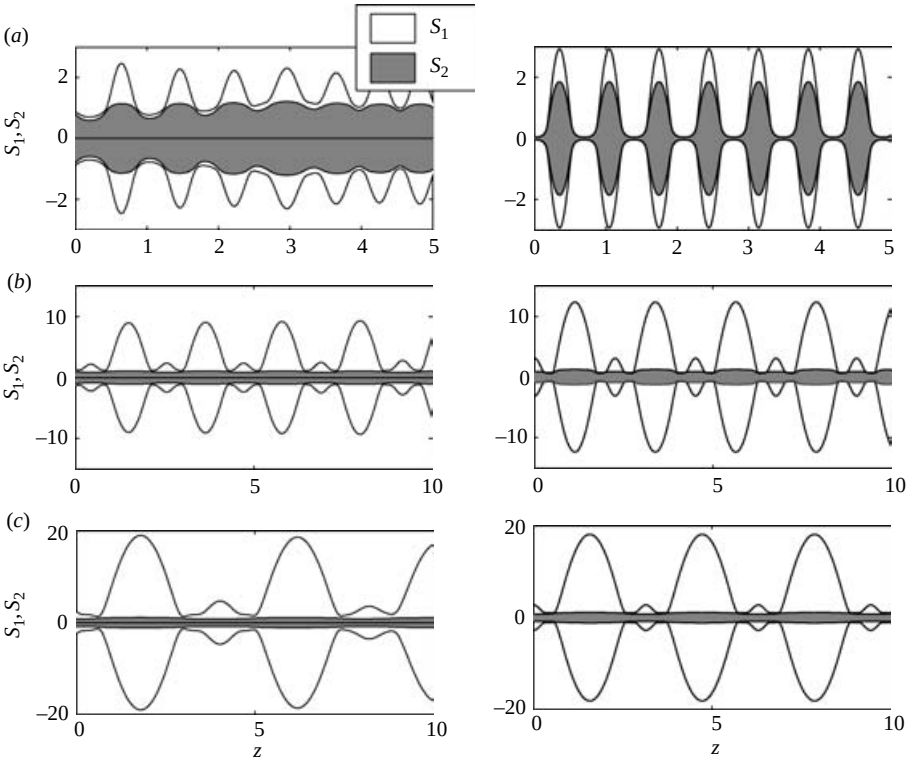

FIGURE 6. The effect of varying α on the evolution of the threads when the core is more viscous than the annulus (shaded region) with $\gamma = M = 1$ and $\epsilon = 0.05$. The left-hand panels show profiles of S_1 and S_2 at $t = 15.7, 4.76, 3.6$ for $\alpha = 1.5, 5$ and 10, respectively. The evolution is initiated by random disturbances taken from a uniform distribution on $[-1, 1] \times 10^{-5}$ introduced to the outer interface. The right-hand panels show analogous profiles for simulations initiated by solutions to the linearized equations associated with the most dangerous stretching mode, which corresponds approximately to $k = 9$, 2.8 and 1.4 for (*a*) $\alpha = 1.5$, (*b*) 5 and (*c*) 10 (see figure 2), respectively, imposed upon the outer interface; the amplitude of the initial disturbance is 10^{-5}. Here, the times are $t = 19.7, 7.1, 4.7$ for $\alpha = 1.5, 5$ and 10, respectively.

I, in which both interfaces moved synchronously owing to the radial independence of the axial velocity component. The computations continue until the outer and inner interfaces are separated by a distance of $O(10^{-4})$; this is referred to below as 'pinch-off' or 'breakup' although it should be noted that this does not mean that the interfaces eventually touch. This appears to take place before the radius of the viscous core itself has had an opportunity to achieve similar values for all the parameters examined in the present work. It should also be pointed out, however, that the dynamics in the present case are markedly different from that of a single thread or of a compound thread wherein the core breaks up first. In the latter cases, the curvature and axial velocities diverge as breakup is approached. In the present case, the velocities remain finite (as shown in figure 9), and the interfaces approach one another via a fluid 'drainage' mechanism rather than a catastrophic event. Note that had intermolecular forces been included in our model, then finite-time pinch-off would have occurred.

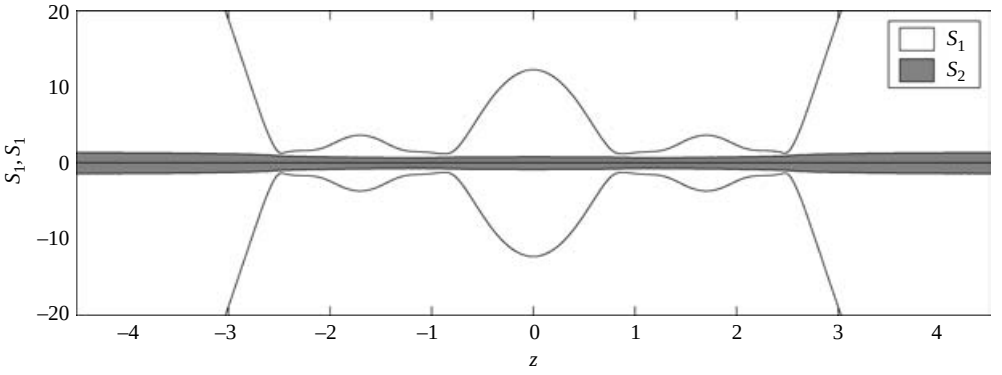

FIGURE 7. Multiple satellite formation when the core is more viscous than the annulus with $\alpha = 20$, initiated by the most dangerous mode: $k_{max} = 0.699$ with remaining parameters the same as figure 6: $t_f = 4.8$.

The trend observed in figure 6 is that for small α we have a thin outer, less viscous, annulus that rapidly forms small isolated regions separated by a very thin film. Increasing α leads to regular periodic disturbances with large 'rings' of fluid separated by smaller ones. That is, the evolution of the annulus is accompanied by multiple 'satellite' formation for sufficiently large α (see figure 7). These smaller intermediate fluid regions eventually split further to generate multiple satellites, although this may lie outside the limits of applicability of the current theory, which is strictly valid for $\epsilon\alpha \ll 1$. There is also a minimal satellite size as predicted by our linear stability analysis, so we have qualitative agreement with the predictions of linear theory.

It is interesting to contrast the evolution of the thread starting from different initial conditions. Except for the smallest values of α considered, the final profiles associated with the initially pseudo-random perturbations appear to be qualitatively and quantitatively similar to those associated with the most dangerous linear forcing with minor differences occurring in the isolated smaller droplets regions. This is not surprising since, as shown in figure 8(a), rapid organization occurs of the initial pseudo-random disturbances into the most dangerous mode for $\alpha = 5$, $\gamma = M = 1$ and $\epsilon = 0.05$ that corresponds to $k_{max} = 2.8$; thus memory of the initial conditions is quickly erased. Figure 8(b) shows a comparison of the prediction of linear theory and that of the numerical computations. Inspection reveals excellent agreement at early times prior to the onset of nonlinearities and inspires confidence in the performance of the numerical procedure. For relatively large values of α, the initial evolution is as predicted by linear theory: in-phase interface evolution. Nonlinearity then gives rise to satellite formation and the interfaces can then move out-of-phase; cf. figure 6(c). Thus linear theory cannot be entrusted to predict the ultimate fate of the compound thread.

For smaller α values, it appears that the time to 'pinch-off' occurs less rapidly starting from linear forcing; the growth rates for the most dominant mode decrease with decreasing α. This allows both the core and the annular region to deform, promoting the possibility of thread 'breakup' into compound drops for sufficiently small α, rather than annular drops on the surface of the highly viscous core. This behaviour, however, was not observed for the smallest α values used when $\gamma = 1$; 'breakup' in the annular regime occurred first.

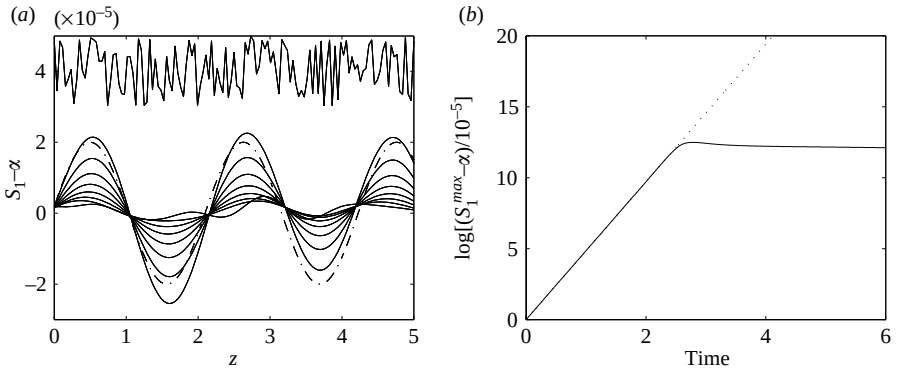

FIGURE 8. Comparisons with linear theory for the highly viscous annular case with $\alpha = 5$: (*a*) shows the early-time evolution of profiles initiated with pseudo-random disturbances with the initial profile shown displaced by 4×10^{-5} and the first eight profiles separated in time by 8×10^{-3} showing evolution towards the most unstable stretching mode as predicted by linear theory. This most unstable mode is shown as the dot-dashed line with amplitude chosen for aesthetic comparison. (*b*) shows the growth measure calculated from the numerical simulations (solid line) versus the growth rate from linear theory (dotted line) (equal to $\lambda_{max} = 4.85$ in this case). The rest of the parameters are $\gamma = M = 1$, $k_{max} = 2.8$ and $\epsilon = 0.05$.

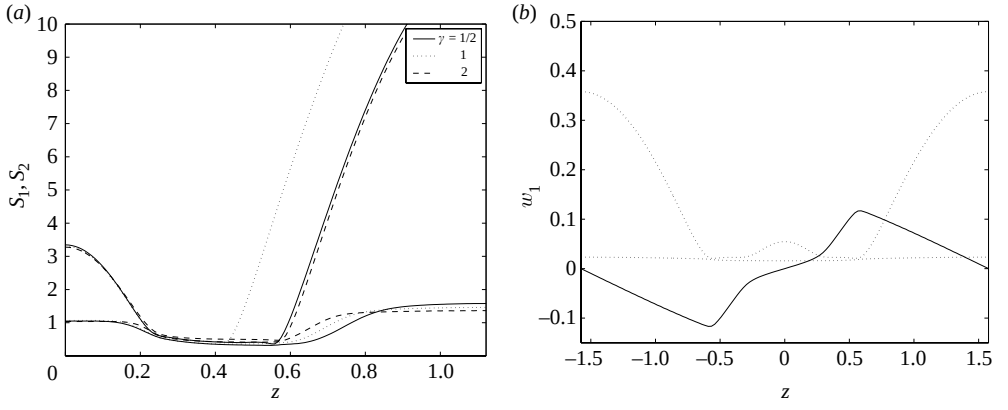

FIGURE 9. (*a*) The variation of interface positions with γ for $\alpha = 5$, initiated by the most dangerous mode: $k_{max} = 2.77, 2.78$ and 2.79 for $\gamma = 1/2, 1, 2$ with the remaining parameters the same as figure 6: $t_f = 12.6, 7.1$ and 3.8. (*b*) shows the axial velocity w_1 for the $\alpha = 10$ computation of figure 6 initiated by the most dangerous mode. The dotted lines show the interface positions (divided by 50) for reference.

Variation with γ has a relatively weak effect upon the satellite size, but can dramatically affect the time to 'pinch-off'; this can be observed from the increasing growth rates with γ from linear theory. Figure 9 shows some typical profiles when $\alpha = 5$. Physically, as we decrease γ, we demote the influence of the outer less viscous fluid and the flow becomes dominated by the highly viscous core. Indeed, as $\gamma \to 0$, we tend towards the conventional single jet (cf. §2.1.2) and pinch-off then occurs in the central highly viscous core. We turn our attention now to the case of highly viscous annuli.

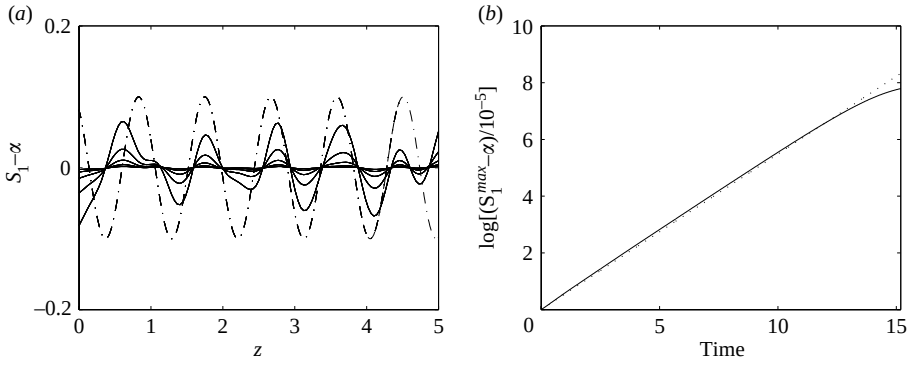

FIGURE 10. Comparisons with linear theory when the core is less viscous than the annulus with $\alpha = 2$: (*a*) shows the early-time evolution of profiles initiated with pseudo-random disturbances. Here, four profiles are shown at $t = 8, 9, 10, 11$ illustrating the evolution towards the most unstable stretching mode as predicted by linear theory, shown as the dot-dashed line with amplitude chosen for aesthetic comparison. (*b*) shows the growth measure calculated from the numerical simulations (solid line) versus the growth rate from linear theory (dotted line) (equal to $\lambda_{max} = 0.55$ in this case). The rest of the parameter values are $\gamma = M = 1$, $k_{max} = 6.83$, $\epsilon = 0.05$.

4.2. *Highly viscous annulus*

Here, we describe the results of the simulations for the highly viscous annulus case. The same numerical scheme briefly described in § 4 is again used in this case. In figure 10, we show a comparison of the predictions of linear theory with numerical solutions starting from initial pseudo-random forcing. In figure 10(*a*), rapid organization of the random perturbations occurs into coherent structures, which quickly begin to resemble the most dangerous linear mode, which is a stretching mode. From figure 10(*b*), it becomes clear that the numerical solution starting from this mode is in excellent agreement with the linear theory predictions, and that the interfaces move in-phase, prior to the onset of nonlinearities. This inspires further confidence in the predictions of the numerical procedure used in this study.

Typical numerical simulations are shown in figure 11, in which we illustrate the effect of increasing α on S_1 and S_2 with $\gamma = 1$ starting from pseudo-random initial forcing. For small α values, the core assumes a 'bamboo-shoot' type of structure and the thin annulus 'pinches off' first, in spite of it being more viscous than the core region. This is because the rapid deformation of the core causes the relatively thick regions of the core to interact with the annulus, which exhibits a much slower response. These interactions give rise to 'pinch-off' of the annulus, which is, once again, a short-hand interpretation of $S_1 - S_2 \sim O(10^{-4})$. We also remark that out-of-phase interface motion contradicts the predictions of the linear stability analysis, which further demonstrates the short-comings of linear theory in predicting the ultimate fate of a compound thread in the nonlinear regime.

In figure 12, we show analogous plots to those shown in figure 11, but here the solutions were generated starting from linear mode forcing. In this case, the profiles appear to be similar, but much more regular with the core undergoing 'breakup' into droplets, exhibiting a 'string of pearls' type of structure, particularly for relatively large α values. The viscous annulus, on the other hand, undergoes relatively mild deformations for these α values.

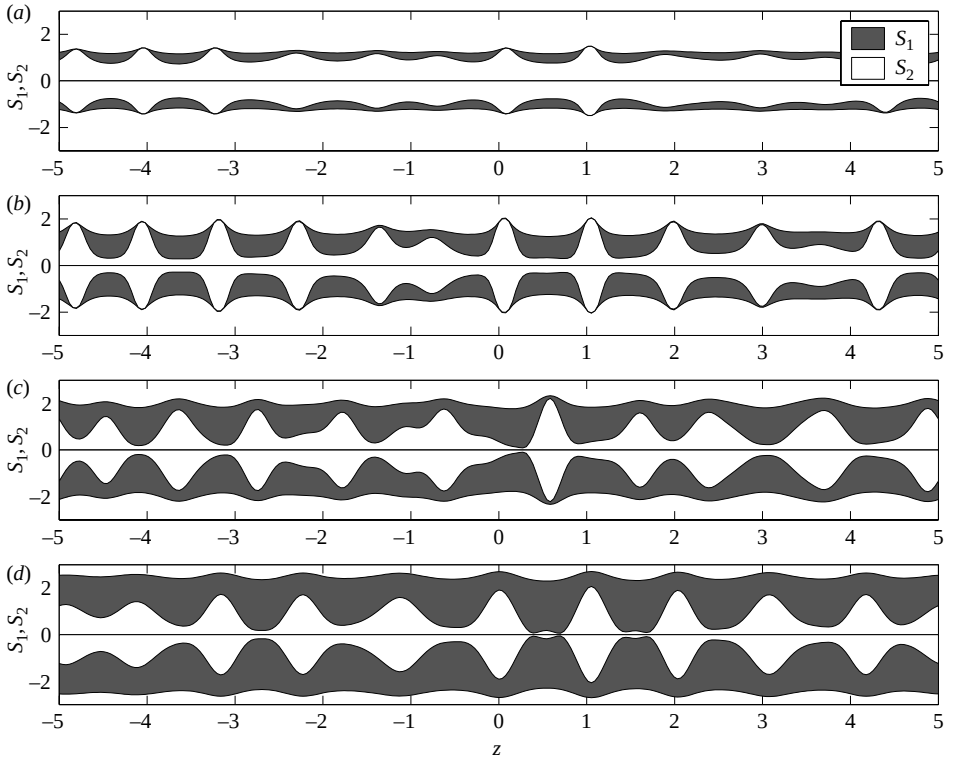

FIGURE 11. The effect of varying α on the evolution of the threads when the core is less viscous than the annulus (shaded region) with $\gamma = M = 1$ and $\epsilon = 0.05$. Here, profiles of S_1 and S_2 are presented at (*a*) $t = 7.4$, (*b*) 14.5, (*c*) 23 and (*d*) 27.4 for $\alpha = 1.25, 1.5, 2$ and 2.5, respectively. The evolution is initiated by pseudo-random disturbances taken from a uniform distribution on $[-1, 1] \times 10^{-4}$ introduced to the outer interface.

Thus increasing the relative thickness of the highly viscous annulus progressively increases the likelihood of 'breakup' of the less viscous core; an example of this situation is shown in figure 11(*d*). However, in the $\alpha = 2.5$ case, wherein core breakup occurs, the curvature of the inner interface diverges. This is most easily seen by inspecting the pressure in the core, p_2 (see figure 13) which clearly diverges as $S_2 \to 0$ (see (2.68)) which occurs in the $\alpha = 2.5$ case. This is in stark contrast to the behaviour at smaller α values where both interfaces simply collide. Note also that the axial velocities remain finite in the highly viscous annulus case for all the α values examined and that pinch-off occurs via a 'drainage' mechanism rather than through the divergence of the axial velocity.

We have also examined the effect of varying γ on the dynamics; this is shown in figure 14 for $\alpha = 1.5$, and again has a relatively weak effect upon the satellite size. The satellite sizes do lengthen slightly with increasing γ. The time to 'pinch-off' decreases as γ increases; this can be observed from the increasing growth rates with γ from linear theory.

5. Concluding remarks

In this paper, we have examined the evolution of compound threads, which are composed of fluids having sharp viscosity (and density) contrasts. Two particular

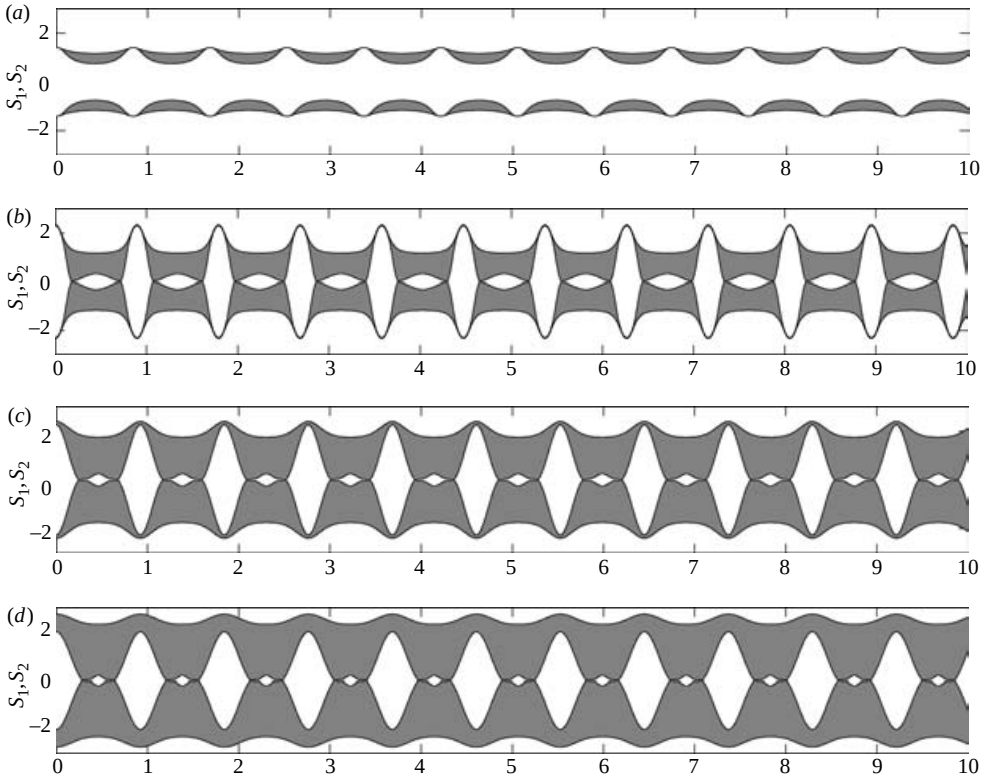

FIGURE 12. The effect of varying α on the evolution of the threads having a highly viscous annulus (shaded region) with $\gamma = M = 1$ and $\epsilon = 0.05$. Here, profiles of S_1 and S_2 are presented at (*a*) $t = 5$, (*b*) 12.1, (*c*) 15.1 and (*d*) 16.6 for $\alpha = 1.25$, 1.5, 2 and 2.5, respectively. The evolution is initiated by solutions to the linearized equations associated with the most dangerous mode, which corresponds approximately to $k = 7.46, 7.02, 6.83$ and 6.82 for $\alpha = 1.25, 1.5, 2$ and 2.5 (see figure 4), respectively, imposed upon the outer interface; the amplitude of the initial disturbance is 10^{-4}.

cases were examined: a highly viscous core surrounded by a much less viscous annular fluid, and a highly viscous annulus, which encloses a much less viscous core. The more viscous fluid was also assumed to be much denser than the other fluid. This allowed the retention of inertial contributions in the more viscous phase, which may not be physically realizable but, nevertheless, allowed the recovery of many of the equations governing the evolution of jets and threads published in the literature. In fact, the model systems of equations deduced here reduce, in appropriate limits, to several special cases, notably to the equations of Hammond (1983), Eggers (1993) and Sierou & Lister (2003).

A long-wave theory valid for slender threads was used to derive evolution equations for the interfacial locations and axial velocities of the more viscous regions; in the highly viscous annulus case, an equation for the pressure in this region was also solved. The approach adopted in this paper is similar to that employed by paper I, wherein the nonlinear stability of compound threads was also examined. The assumption underlying their analysis, however, was that the viscosity ratio was of order unity, which rendered the axial component of the velocity field radially independent. This

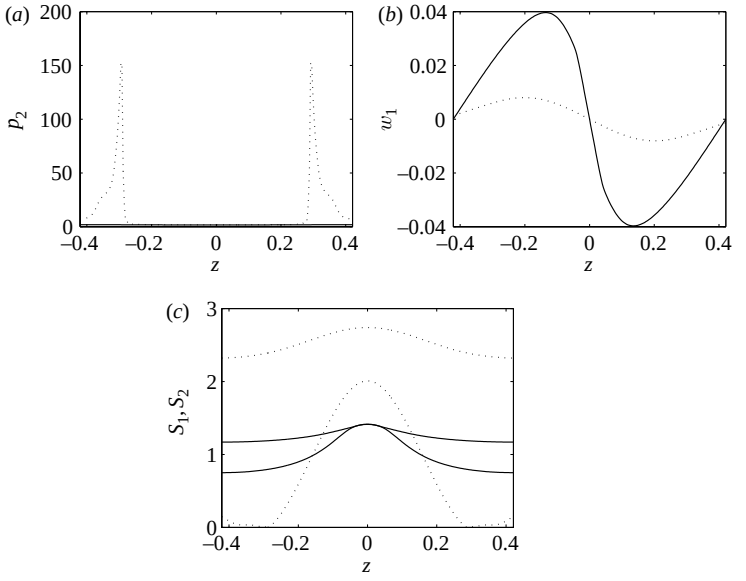

FIGURE 13. The pressure and velocity profiles for $\alpha = 1.25$ (solid) and $\alpha = 2.5$ (dotted) for the profiles shown in figure 12. (c) The interface positions.

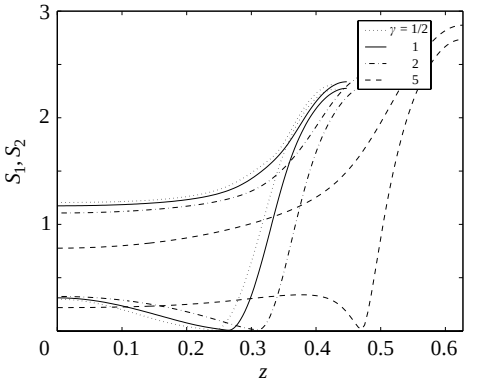

FIGURE 14. The variation of S_1, S_2 with γ for $\alpha = 1.5$, initiated by the most dangerous mode: $k_{max} = 7.31, 7.02, 6.42$ and 5 for $\gamma = 1/2, 1, 2$ and 5 with remaining parameters the same as figure 11: $t_f = 14.3, 12.1, 11$ and 9.1.

resulted in simultaneous breakup of the core and annular regions regardless of their initial thickness ratio, α.

The linear stability characteristics of the threads were then analysed for the two chosen cases of a highly viscous core and annulus. In both cases, two unstable modes were identified: a stretching and a squeezing mode, which correspond to interfacial motion in- and out-of-phase, respectively. In all cases examined, the stretching mode was found to be the dominant mode of linear growth, in agreement with previous work on compound jet stability (Chauhan *et al.* 1996, 2000). We have also found that decreasing the relative thickness of the more viscous fluid, and/or increasing the ratio of interfacial tensions of the outer to inner fluids, γ, leads to more unstable situations.

The stability of the threads in the nonlinear regime was then investigated via transient numerical solutions of the evolution equations for a wide range of parameters. A numerical procedure based on spectral discretization of spatial derivatives and Gear's method in time was employed to carry out the computations. Solutions were obtained starting from either pseudo-random perturbations or the most dangerous linear mode; excellent agreement with the predictions of linear theory was obtained in each case.

The numerical results show that in the highly viscous core case, the annular region undergoes breakup into either small droplets of nearly uniform size, or larger drops separated by droplets of smaller size depending on the magnitude of α; multiple satellites were also observed for large α values. It is notable that, in the nonlinear regime, the interfaces can move out-of-phase and this is contrary to the prediction that we obtain from linear theory. In the highly viscous annulus case, breakup of either the annular or core regions is possible for small and large α values, respectively. In the former limit, the thread assumes a 'bamboo-shoot' type of shape, while in the latter, the core region exhibits a 'string-of-pearls' shape. Increasing γ was found to decrease the time to pinchoff; the satellite size, however, was found to be relatively insensitive to γ variations.

D. T. P. thanks the National Science Foundation for support under grant DMS-0072228. We are grateful to the referees for several useful and interesting suggestions.

REFERENCES

Ambravaneswaran, B. & Basaran, O. A. 1999 Effects of surfactants on the nonlinear deformation and breakup of stretching liquid bridges. *Phys. Fluids* **11**, 997–1015.

Ambravaneswaran, B., Wilkes, E. D. & Basaran, O. A. 2002 Drop formation from a capillary tube: comparison of one-dimensional (1-d) and two-dimensional (2-d) analyses and occurrence of satellite drops. *Phys. Fluids* **14**, 2606–2621.

Brenner, M. P., Shi, X. D. & Nagel, S. R. 1994 Iterated instabilities during droplet fission. *Phys. Rev. Lett.* **73**, 3391–3394.

Burlak, G., Koshevaya, S., Sanchez-Mondragon, J. & Grimalsky, V. 2001 Electromagnetic eigenoscillations and fields in a dielectric microsphere with multilayer spherical stack. *Opt. Commun.* **187**, 91–105.

Chandrasekhar, S. 1961 *Hydrodynamic and Hydromagnetic Stability*. Oxford University Press.

Chauhan, A., Maldarelli, C., Papageorgiou, D. & Rumschitzki, D. 2000 Temporal instability of compound jets and threads. *J. Fluid Mech.* **420**, 1–25.

Chauhan, A., Maldarelli, C., Rumschitzki, D. & Papageorgiou, D. 1996 Temporal and spatial instability of an inviscid compound jet. *Rheol. Acta* **35**, 567–583.

Chauhan, A., Maldarelli, C., Rumschitzki, D. & Papageorgiou, D. 2003 An experimental investigation of the convective instability in a jet. *Chem. Engng Sci.* **58**, 2421–2432.

Chen, A. U., Notz, P. K. & Basaran, O. A. 2002 Computational and experimental analysis of pinch-off and scaling. *Phys. Rev. Lett.* **88**, art. no. 174501.

Craster, R. V., Matar, O. K. & Papageorgiou, D. T. 2002 Pinchoff and satellite formation in surfactant covered viscous threads. *Phys. Fluids* **14**, 1364.

Craster, R. V., Matar, O. K. & Papageorgiou, D. T. 2003 Pinchoff and satellite formation in compound viscous threads. *Phys. Fluids* **15**, 3409–3428.

Denn, M. M. 1980 Drawing of liquids to form fibers. *Annu. Rev. Fluid Mech.* **12**, 365.

Doshi, P., Cohen, I., Zhang, W. W., Siegel, M., Howell, P., Basaran, O. A. & Nagel, S. R. 2003 Persistence of memory in drop breakup: the breakdown of universality. *Science* **302**, 1185–1189.

Eggers, J. 1993 Universal pinching of 3D axisymmetric free-surface flow. *Phys. Rev. Lett.* **71**, 3458–3460.

Eggers, J. 1995 Theory of drop formation. *Phys. Fluids* **7**, 941–953.

Eggers, J. 1997 Nonlinear dynamics and breakup of free-surface flows. *Rev. Mod. Phys.* **69**, 865–929.

Eggers, J. & Dupont, T. F. 1994 Drop formation in a one-dimensional approximation of the Navier–Stokes equation. *J. Fluid Mech.* **262**, 205–221.

Hammond, P. S. 1983 Nonlinear adjustment of a thin annular film of viscous fluid surrounding a thread of another within a circular cylindrical pipe. *J. Fluid Mech.* **137**, 363–384.

Hansen, S., Peters, G. W. M. & Meijer, H. E. H. 1999 The effect of surfactant on the stability of a fluid filament embedded in a viscous fluid. *J. Fluid Mech.* **382**, 331–349.

Hardas, N., Danviriyakul, S., Foley, J., Nawar, W. & Chinachoti, P. 2000 Accelerated stability studies of microencapsulated anhydrous milk fat. *Lebensmittel-Wiss. Technol.* (*Food Sci. Technol.*) **33**, 506–513.

Henson, G. M., Cao, D. & Bechtel, S. E. 1998 A thin-filament melt-spinning model with radial resolution of temperature and stress. *J. Rheol.* **42**, 329–360.

Hertz, C. H. & Hermanrud, B. 1983 A liquid compound jet. *J. Fluid Mech.* **131**, 271.

Herzenberg, L. A. & Sweet, R. G. 1976 Fluorescence-activated cell sorting. *Sci. Am.* **234**, 108.

Jung, T., Kamm, W., Breitenbach, A., Kaiserling, E., Xiao, J. & Kissel, T. 2000 Biodegradable nanoparticles for oral delivery of peptides: is there a role for polymers to affect mucosal uptake? *Eur. J. Pharm. Biopharm.* **50**, 147–160.

Kalliadasis, S. & Chang, H.-C. 1994 Drop formation during coating of vertical fibres. *J. Fluid Mech.* **261**, 135–168.

Keller, J. B., Rubinow, S. L. & Tu, Y. O. 1973 Spatial instability of a jet. *Phys. Fluids* **16**, 2052.

Kwak, S. & Pozrikidis, C. 2001 Effect of surfactants on the instability of a liquid thread or annular layer. part i: Quiescent fluids. *Intl J. Multiphase Flow* **27**, 1–37.

Lee, H. C. 1974 Drop formation in a liquid jet. *IBM J. Res. Dev.* **18**, 364–369.

Lee, Y. H., Kim, C. A., Jang, W. H., Choi, H. J. & Jhon, M. S. 2001 Synthesis and electrorheological characteristics of microencapsulated polyaniline particles with melamine–formaldehyde resins. *Polymer* **42**, 8277–8283.

Leib, S. J. & Goldstein, M. E. 1986*a* Convective and absolute instability of a viscous jet. *Phys. Fluids.* **29**, 952.

Leib, S. J. & Goldstein, M. E. 1986*b* The generation of capillary instabilities on a liquid jet. *J. Fluid Mech.* **168**, 479.

Lin, S. P. & Reitz, R. 1998 Drop and spray formation from a liquid jet. *Annu. Rev. Fluid Mech.* **30**, 85–105.

Lister, J. R. & Stone, H. A. 1998 Capillary breakup of a viscous thread surrounded by another viscous fluid. *Phys. Fluids* **10**, 2758–2764.

Mathiowitz, E., Jacob, J., Jong, Y., Carino, G. D. E., Chickering, P. C., Santos, C., Vijayaraghavan, K., Montgomery, S., Bassett, M. & Morrell, C. 1997 Biologically erodable microsphere as potential oral drug delivery system. *Nature* **386**, 410–414.

McKinley, G. H. & Tripathi, A. 2000 How to extract the Newtonian viscosity from capillary breakup measurements in a filament rheometer. *J. Rheol.* **44**, 653–670.

Notz, P. K., Chen, A. U. & Basaran, O. A. 2001 Satellite drops: unexpected dynamics and change of scaling during pinch-off. *Phys. Fluids* **13**, 549–552.

Papageorgiou, D. T. 1995*a* Analytical description of the breakup of liquid jets. *J. Fluid Mech.* **301**, 109–132.

Papageorgiou, D. T. 1995*b* On the breakup of viscous liquid threads. *Phys. Fluids* **7**, 1529–1544.

Papageorgiou, D. T. & Orellana, O. 1998 Study of cylindrical jet breakup using one-dimensional approximations of the Euler equations. *SIAM J. Appl. Maths* **59**, 286–317.

Radev, S. & Shkadov, V. 1985 On the stability of two-layer capillary jet. *Theor. Appl. Mech.* **16**, 68.

Radev, S. & Tchavdarov, B. 1988 Linear capillary instability of compound jets. *Intl J. Multiphase Flow* **14**, 67–79.

Rayleigh, Lord 1878 On the stability of liquid jets. *Proc. Lond. Math. Soc.* **10**, 4.

Renardy, M. 1994 Some comments on the surface-tension driven break-up (or lack of it) of viscoelastic jets. *J. Non-Newtonian Fluid Mech.* **51**, 97–102.

Rothert, A., Richter, R. & Rehberg, I. 2003 Formation of a drop: viscosity dependence of three flow regimes. *New J. Phys.* **5**, art. 59.

Sanz, A. & Meseguer, J. 1985 One-dimensional analysis of the compound jet. *J. Fluid Mech.* **159**, 55–68.

Schulkes, R. M. S. M. 1993*a* Dynamics of liquid jets revisited. *J. Fluid Mech.* **250**, 635–650.

Schulkes, R. M. S. M. 1993*b* Nonlinear dynamics of liquid columns: a comparative study. *Phys. Fluids* A **5**, 2121–2130.

Shi, X. D., Brenner, M. P. & Nagel, S. R. 1994 A cascade of structure in a drop falling from a faucet. *Science* **265**, 219–222.

Shkadov, V. Y. & Sisoev, G. M. 1996 Instability of a two-layer capillary jet. *Intl J. Multiphase Flow* **22**, 35–54.

Sierou, A. & Lister, J. R. 2003 Self-similar solutions for viscous capillary pinch-off. *J. Fluid Mech.* **497**, 381–403.

Timmermans, M.-L. E. & Lister, J. R. 2002 The effect of surfactant on the stability of a liquid thread. *J. Fluid Mech.* **459**, 289.

Tomotika, M. 1934 On the instability of a cylindrical thread of a viscous liquid surrounded by another viscous liquid. *Proc. R. Soc. Lond.* A **150**, 322.

Wilkes, E. D., Phillips, S. D. & Basaran, O. A. 1999 Computational and experimental analysis of dynamics of drop formation. *Phys. Fluids* **11**, 3577–3598.